Spring 3-25-2020

A Polarimetric Radar Analysis of Cold- and Warm-Based Supercells

Timothy J. Gunkel
University of Nebraska - Lincoln, tgunkel1221@huskers.unl.edu

A POLARIMETRIC RADAR ANALYSIS OF COLD- AND WARM-BASED SUPERCELLS

by

Timothy J. Gunkel

A THESIS

Presented to the Faculty of

The Graduate College of University of Nebraska

In Partial Fulfillment of Requirements

For the Degree of Master of Science

Major: Earth and Atmospheric Sciences

Under the Supervision of Professor Matthew Van Den Broeke

Lincoln, Nebraska

May, 2020

A POLARIMETRIC RADAR ANALYSIS OF COLD- AND WARM-BASED SUPERCELLS

Timothy J. Gunkel, M.S.

University of Nebraska, 2020

Advisor: Matthew Van Den Broeke

Polarimetric analyses of supercell thunderstorms have been increasingly common within the past decade, since operational polarimetric radar data became available in 2013. Although polarimetric signatures within supercell thunderstorms are well known, few have investigated variability in these signatures in differing environments. Polarimetric signatures can provide vital information regarding the microphysical characteristics and processes in supercell thunderstorms. Specific polarimetric signatures of interest are the differential reflectivity (Z_{DR}) column, the low-level polarimetrically inferred hail core, and the Z_{DR} arc. These signatures provide information regarding updraft characteristics, hailfall characteristics, and size sorting processes in the storm-relative inflow. Previous studies have identified these signatures and their microphysical significance, yet there is much to learn regarding how these characteristics differ between environments. The investigation of these signatures found within supercells characterized by differing cloud base temperatures will be discussed herein. These preliminary results can serve as an operational aid when observing supercell thunderstorms in a severe weather event, as these signatures can help to determine the potential for specific hazards, given specific environments. The environments of each type of supercell, along with the

characteristics of their associated polarimetric signatures, can provide information about updraft intensity, hailfall characteristics, or tornado potential. This investigation finds that there are some significant differences, especially within the Z_{DR} columns and the low-level polarimetrically inferred hail core, in the observed polarimetric signatures between different environments. All warm-based supercells exhibited a Z_{DR} column, while many of the cold-based cases did not exhibit any column. Along with more warm-based cases exhibiting columns, they were also deeper than those observed in the cold-based cases. Cold-based supercells also exhibited much larger inferred hail cores than the warm-based supercells, which can be attributed to the cooler environments in which cold-based supercells are found. Finally, the Z_{DR} arcs shown no large statistical differences across environments. This could be a consequence to the different thresholds utilized for identifying the arcs, along with different hailfall characteristics between environments.

Acknowledgments

I would like to thank my advisor, Dr. Matthew Van Den Broeke for providing me with the opportunity to study and conduct research as part of his research group at the University of Nebraska—Lincoln, along with providing me with the opportunity to be a part of the Earth Observation for Science, Society, and Sustainability (EOS^3) Graduate Fellowship program. Also, a special thank you to Dr. Matthew Van Den Broeke for working with me and giving great guidance while I was working at my internship in Rapid City, SD, over the summer. Also, thank you to my committee members, Dr. Mark Anderson and Dr. Adam Houston for feedback and guidance through this process.

I would also like to thank my fellow colleagues and friends that I have made within the department. Not only were they very supportive, but they also provided some great advice and resources for aspects of this project.

I would also like to thank the Department of Earth and Atmospheric Sciences for funding me as a graduate teaching assistant for my first year here, which provided great experience in teaching what I love in a classroom setting.

TABLE OF CONTENTS

Acknowledgments ..... **iii**

Chapter 1. Introduction **1**

Chapter 2. Background **4**

a. Supercell Structure 4

b. Supercell Environments 7

c. Dual-Polarization Radar 10

i. Cross-Correlation Coefficient (ρ_{hv}) 12

ii. Differential Reflectivity (Z_{DR}) 13

d. Dual-Polarization Radar Signatures 14

i. Z_{DR} Columns 14

ii. Low-Level Radar-Inferred Large Hail Signatures 18

iii. Z_{DR} Arcs 21

Chapter 3. Data and Methodology **25**

a. Data 25

b. Cases 26

c. Z_{DR} Calibration 30

d. Environmental Characteristics 31

e. Z_{DR} Columns 32

f. Low-Level Radar-Inferred Large Hail Signature 33

g. Z_{DR} Arc 35

Chapter 4. Results **37**

a. Environmental Variability 37

b. Z_{DR} Columns 43

c. Low-Level Radar-Inferred Large Hail Signature 49

d. Z_{DR} Arcs 53

Chapter 5. Conclusions **59**

Chapter 6. References **66**

1. Introduction

Supercell thunderstorms have been investigated extensively in the past several decades because these storms have a relatively high impact and a high likelihood of accompanying severe weather (e.g., Marwitz 1972; Moller et al 1994; Kumjian and Ryzhkov 2008; Van Den Broeke 2016). Compared to other forms of convection (single cell, multicell, squall line, etc.), supercells lead to an unproportionate amount of damage. Supercells can produce large hail, flooding rains, and/or strong tornadoes. The overall structure of the supercell and the associated environments in which they reside in are relatively well known. Both the structure and environment can differ significantly between supercells, where the overall environmental profile is a large factor in the structure of a supercell. The environment, and therefore the structure, can also assist in the determination of which type of the above-mentioned hazards can be expected in a given scenario.

Polarimetric radar studies on supercell thunderstorms have grown fairly common, especially once dual polarization data became operationally available in 2013 throughout the conterminous United States. Several studies have utilized the new polarimetric radar variables to identify different microphysical processes and characteristics through the identification of polarimetric radar signatures (e.g. Kumjian and Ryzhkov 2008, 2009, 2012; Dawson et al. 2014; Van Den Broeke 2016). Through the identification of these signatures, microphysical aspects, such as hydrometeor orientation and phase, can be determined with better accuracy than could have been done in the past. Along with these microphysical characteristics, details regarding updraft characteristics, hailfall, tornado

potential, and hydrometeor size sorting processes can be determined through polarimetric analysis. Understanding changes in the orientation of polarimetric signatures can lead to information regarding the current state of the storm, along with the potential determination in how the storm will progress (strengthening and weakening phases).

The goal of this research is to analyze common polarimetric signatures noted in prior literature, with a specific focus on investigating how these polarimetric signatures differ between two environments on opposite sides of an environmental parameter space, cold- and warm-based environments. Although a few studies have investigated microphysical processes within supercells in different environments, there is still much to learn (Thompson et al. 2003; Van Den Broeke 2016). In this investigation, cold-based supercells are defined as supercells that develop in an environment characterized by cloud base temperatures 5 ℃ or cooler, while warm-based supercells develop in environments with cloud base temperatures 15 ℃ or warmer (Van Den Broeke et al. 2008). Along with the environmental criteria, each supercell case had to be relatively isolated from other convection, that way each signature could be observed as clearly as possible. It was noted that supercells found in the Southern Plains are more likely to be warm-based, compared to those found in the High Plains (cold-based). Although these circumstances hold true for many cases, the locations do not define which type of supercell is present. A similar study was completed by Van Den Broeke (2016) in which the polarimetric signatures were investigated as a function of similar and different environmental characteristics, although no set environmental criteria were utilized. The findings of the current investigation can serve as an aid in the operational setting,

especially when determining the current state of an ongoing supercell and messaging the potential hazards. Understanding polarimetric signatures common in specific environments can aid in hazard messaging prior to or during a severe weather event. This analysis also focuses on the strong environmental differences between supercell types, with hopes that this would persuade forecasters to really dive into the environmental data and models available to better determine hazard potential based on these two supercells in very different environments. Given the lack of research investigating common polarimetric signatures and their differences between supercell environments, this investigation will be completed to help fill in the knowledge gap on supercells in differing environments. The hypotheses of this study are as follows:

1. Z_{DR} columns will exhibit greater depth and a larger areal extent in warm-based supercell environments since these environments will generally have higher MUCAPE, leading to stronger vertical motions.
2. Low-level Z_{DR} inferred large hail signatures will cover a larger areal extent in cold-based supercells due to their higher and cooler cloud bases and because of their cooler conditions through a deep layer, allowing the formation of more ice particles, ultimately leading to more hail.
3. Z_{DR} arcs will exhibit a larger areal extent in warm-based supercells, partially due to higher environmental MUCAPE and SREH, yielding stronger rotating updrafts. These stronger updrafts will enhance the size sorting within the forward flank of the supercells, leaving larger raindrops there while the smaller raindrops are more readily advected towards the updraft region and into the storm core.

2. Background

a. Supercell Structure

Supercell thunderstorms are deep convective storms that contain a strong and persistent rotating updraft, known as a mesocyclone, along with two downdraft regions (Lemon and Doswell 1979). A mesocyclone is a rotating updraft region within the supercell thunderstorm and stretches through much of the storm's depth with strong vertical velocities that can last for long periods of time (Moller et al. 1994). Supercells can also exhibit other characteristics including a "steady-state" appearance, V-shaped reflectivity notch, bounded weak echo region (BWER), hook echo, inflow notch, and deviant motion (Browning and Donaldson 1963; Lemon 1977; Thompson et al. 2003). Deviant motion occurs when storms propagate to the right (left) of the mean wind, caused by cyclonic (anticyclonic) rotation within the storm (Bunkers et al. 2000). Supercell thunderstorms are common in the central United States; however, past studies have also observed supercells in many other locations outside of the United States (Dessens and Snow 1989; Moller et al. 1994).

Below is a basic schematic developed by Moller et al. (1994) of the supercell radar reflectivity structure based on his observations, along with the outline of the clouds that would be generally depicted through satellite observations (Figure 1). This schematic shows the generalized regions of where rain, hail, the flanking line, the outflow and gust frontal regions, and the convective updraft can be observed.

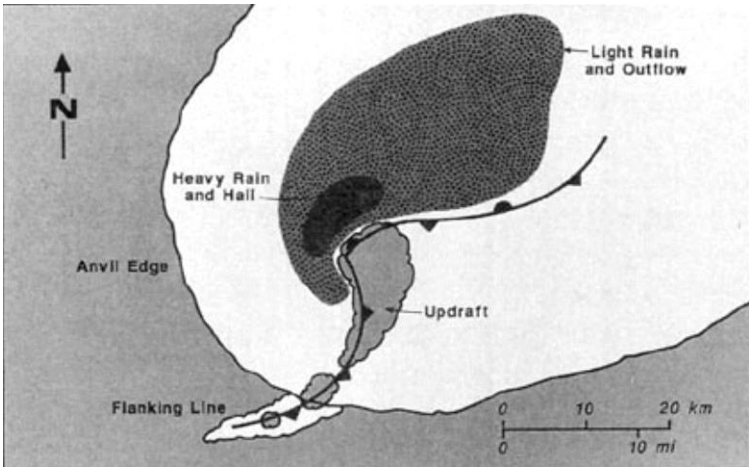

Figure 1. Schematic of a supercell thunderstorm that indicates the generalized locations of hail and rain, along with a few common features of supercells (Moller et al. 1994).

Bunkers et al. (2006a) described supercell thunderstorms as the most severe, organized, and longest-lived mode of isolated deep convection, often lasting in excess of 2 hours. Supercells can become long-lived due to their persistent rotating updraft and strong deep-layer shear, which acts to stop precipitation from falling through the updraft and causes hydrometeors to advect away from the updraft core (Bunkers et al. 2006b). Long-lived supercells are defined to last for four hours or longer, while short-lived supercells are those that last for two hours or less (Bunkers et al. 2006a). Bunkers et al. (2006b) observed a few supercells that lasted longer than 9.5 hours. The above-mentioned characteristics of a supercell are good indicators of rotation in a thunderstorm when velocity data are not available (Bunkers et al. 2006a). They also discussed different convective modes in which supercells can be observed, which include linear, discrete, or mixed. Linear convective modes occur when supercells are found embedded or attached to linear convection, specifically when supercells share a common region of 35 dBZ reflectivity. Discrete supercells are observed when they are in complete isolation from

other convection, or at least a whole storm width apart from one another. Finally, the mixed mode is when supercells fall between the two modes described above. For example, a supercell would be considered to be in mixed mode if it is observed within a very close proximity to a line of convection. Depending on the mode of supercell expected for a given event, knowledge of the mode can provide guidance in forecasting specific hazards (hailfall or tornado potential).

The mesocyclone sets supercells apart from other modes of convection (Browning and Donaldson 1963). Brown (1992) discussed how to identify the mesocyclone using Doppler velocity, which is simply looking for a region of opposing wind velocities that indicate a cyclonic or anticyclonic motion in the velocity field. Burgess et al. (1982) required supercells to exhibit a rotational velocity of at least 25 m s^{-1}. Donaldson (1970) discussed that the mesocyclone should also exhibit temporal and vertical continuity.

Research conducted by Klemp et al. (1981) investigated the structure of supercell thunderstorms, as well as the air and precipitation trajectories observed within. They found that the supercell's updraft generally rose anticyclonically within the storm. This finding led to the conclusion that the orientation of the rotation in a supercell thunderstorm has an association with the storm-relative environmental winds. Entrainment of the environmental air can lead to different air parcel trajectories within the updraft region, where the flow within a specific layer of the updraft is strongly influenced by the direction from which the air was entrained. Precipitation trajectories within a supercell were also found to play an important role in the supercell's longevity. Their observations shown that as rain falls out of a supercell, it falls cyclonically into the

downdraft region, which is opposite the sense of rotation observed in the updraft. The downdrafts produced by the storm are important in maintaining the supercell because the outflow is an important factor in inducing convergence along the gust front, which helps to supply warm and moist air to the updraft of the parent supercell (Klemp et al. 1981). The authors conclude that future research will be needed to investigate the influence of environmental variability on supercell structure, since many different factors (forcing mechanisms, natural variations, and modifications from nearby storms) may lead to different structures than those observed in their research.

b. Supercell Environments

Supercells thrive in environments that support deep moist convection, including ample moisture, a strong lifting mechanism, strong vertical shear, and high helicity values (Moller et al. 1994). Kumjian and Ryzhkov (2008) determined that supercells that form in an environment with a strong veering profile, a clockwise turning of the wind with increasing height (indicating warm air advection), have a higher probability of becoming severe, and may be associated with higher amounts of storm-relative environmental helicity (SREH). SREH is important for supercell thunderstorms because it is a measure of a storm's ability to induce midlevel rotation through the ingestion of streamwise vorticity. Brown (1992) noted that hodographs generated from rawinsonde measurements in supercell environments show a veering wind profile in the lowest 3 km, with winds veering about 90°. These veering winds are shown by hodograph curvature, which indicates streamwise vorticity that is generated in the low levels of the atmosphere and is ingested into the storm inflow, likely inducing midlevel rotation. Hodographs are

helpful for determining the potential for mesocyclone development in convection, leading to formation of supercells. Long or curved hodographs are good indications that there is shear in the environment, leading to a supportive wind profile to form mesocyclones, although these profiles are not required for the generation of a mesocyclone (Markowski and Richardson 2010). The vertical vorticity and velocity, as well as the helicity, are important in forecasting the supercell potential at a given location because they provide important information regarding the vertical forcing within the environment, as well as the rotational potential within the atmosphere. Supercells are also known to form in highly variable convective available potential energy (CAPE) environments (e.g., Moller et al. 1994; Thompson et al. 2003; Bunkers et al. 2006b).

Bunkers et al. (2006b) investigated supercell thunderstorm longevity as a function of different environmental parameters. They found that long-lived supercells are generally found in environments that are supportive of strong tornadoes, specifically with a lower mixed layer lifting condensation level (MLLCL) and a higher SREH value in the 0-1 km layer. Vertical shear was also found to play an important role in the longevity of supercells, where longer-lived supercells were found in environments with strong vertical wind shear, which helps to prevent weaker convection. It was also found by Ferrier and Houze (1989) that tilted updrafts play an important role in updraft intensity and longevity. Tilting allows the updraft to last longer because precipitation loading within the updraft is less of a contributor compared to a vertically stacked updraft, since the slope of the updraft would allow precipitation to fall away from it. Supercell motion can also lead to the enhancement or demise of a supercell, depending on how the supercell

propagates along a boundary or what type of environment it moves into. Specifically, Bunkers et al. (2006b) found that supercells propagating parallel to a boundary or moving into the warm sector of a midlatitude cyclone, characterized by higher heat and moisture content, have a higher probability of becoming long-lived, compared to supercells that travel across a boundary and into less supportive environments (cool and dry), likely becoming more elevated.

Parker (2014) investigated soundings taken near supercells during the Verification of the Origins of Rotation in Tornadoes Experiment (VORTEX2) field campaign, and utilized these data to analyze the similarities and differences between environmental soundings taken ahead of the supercell's inflow region and within the inflow region. The authors also sought to determine if there were any storm modifications to the environment. Soundings were also taken within the outflow region of the storms. Starting from the distant area of the supercell inflow, the CAPE was observed to be relatively high, around 2000 J kg^{-1}, with relatively lower convective inhibition (CIN), around -20 J kg^{-1}. As the soundings were gathered closer to the supercell in the inflow region, the CAPE and lifting condensation level (LCL) heights gradually decreased and the CIN increased, generally caused by the shallow layer of cooling near the surface because of feeder cloud or anvil shading. Faster wind speeds and a backing wind profile was observed in the soundings closest to the storm in the inflow region (at the 0-1 km layer), while a backing profile with lighter winds was observed in the environments farther from the storm. These wind profiles were different than those discussed in prior literature (e.g.,

Brown 1992; Bunkers et al. 2006b); however, Parker (2014) noted that this may be a modification to the environment due to the supercell.

Supercells are known to form as both surface-based and elevated convection. Elevated convection forms in environments with a stable layer at the surface and an unstable layer aloft (e.g., Colman 1990a, b). Macintosh and Parker (2017) also defined elevated convection as a storm that ingests its inflow from above the near-surface layer (>500 m above ground level [AGL]). With a stable layer at the surface, surface-based CAPE will be about 0.0 J kg^{-1}. With a stable surface, some mechanism is needed to force air parcels upward into the unstable layer aloft and to the level of free convection (LFC). Forcing at higher elevations within the unstable layer is also a way to form elevated convection, where forcing from the surface is not required for convection. Mechanisms that can trigger elevated convection include frontal lift, gravity currents interacting with boundaries, or lifting by gravity waves (Rotunno et al. 1988; Carbone et al. 1990; Moore et al. 1998).

c. Dual-Polarization Radar

One of the more recent and noteworthy upgrades to the Weather Surveillance Radar – 1988 Doppler (WSR-88D) network in the United States was the upgrade to dual-polarization capabilities. This upgrade to the radar network allows meteorologists to observe both meteorological and non-meteorological targets through the use of several polarimetric variables with much greater accuracy than was possible prior (Heinselman and Ryzhkov 2006; Van Den Broeke et al. 2008). Dual-polarization radar measures radar variables which are a function of the horizontal and vertical polarizations, which can

provide insight into several physical properties of the scatterers in a volume. Radar reflectivity in the horizontal polarization (Z_{HH}) is a common radar metric that has been used for decades and measures the total backscatter cross-section of a given sample of targets (Rinehart 2010). Z_{HH} is a measure of the total power returned from a sample volume and is measured in dBZ (Rinehart 2010). Aside from radar reflectivity, the new variables are differential reflectivity (Z_{DR}), cross-correlation coefficient (ρ_{hv}), linear depolarization ratio (LDR), and specific differential phase (K_{DP}; Balakrishnan and Zrnić 1990; Ryzhkov and Zrnić 1996). For the interests of this research, only Z_{DR} and the ρ_{hv} will be discussed further. These new observing strategies provide information regarding whether targets are meteorological, along with determining the orientation (shape and size) and phase of the targets (e.g. Heinselman and Ryzhkov 2006; Dawson et al. 2014). Utilizing dual-polarization radar data can also provide information regarding microphysical properties and characteristics of meteorological phenomena. The three polarimetric signatures that will be the focus of this investigation are the Z_{DR} column, low-level polarimetrically-inferred large hail signature, and the Z_{DR} arc. These signatures will be used as proxies to describe the microphysical characteristics and processes occurring within supercells in differing environments. A schematic adapted from Dawson et al. (2014) depicts several polarimetric signatures and where they can be observed within a supercell thunderstorm (Figure 2). The specific thresholds in the schematic are the values found in that investigation, while other thresholds have been used in other studies and will be discussed in following subsections.

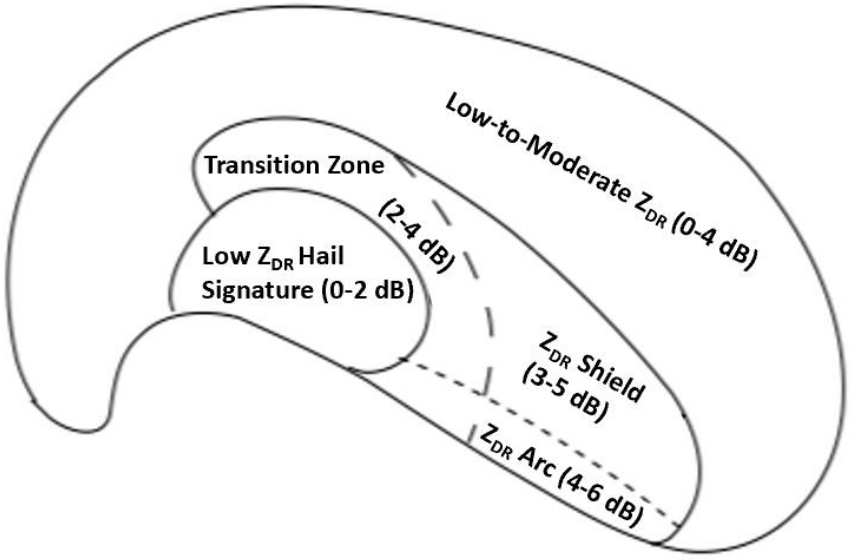

Figure 2. Schematic of a supercell thunderstorm overlaid with the generalized locations of the common polarimetric signatures, along with their respective thresholds (adapted from Dawson et al. 2014).

i. Cross-Correlation Coefficient (ρ_{hv})

The cross-correlation coefficient (ρ_{hv}) is defined by Balakrishnan and Zrnić (1990) as the correlation of the horizontally- to vertically-polarized waves within a distribution of hydrometeors. They describe this variable as a differential phase shift between the horizontal and vertical waves due to scattering, caused by the average size and shape of the hydrometeors in the distribution. When analyzing a sample volume of homogeneous raindrops, the ρ_{hv} of the sample will be ~1.0 because the drops in the volume are uniform. If different sized drops are introduced to the volume, the ρ_{hv} will decrease slightly. They also discuss that whenever there are more raindrops that are largely oblate or prolate, the ρ_{hv} will also decrease to values <1.0. WDTD (NOAA 2018) discuss that large hailstones (>2") produce low ρ_{hv} (generally <0.90), with the ρ_{hv} values reaching <0.75 in spiky hail.

Large hailstones may exhibit a nonuniform appearance such as protuberances, which can yield hail in a volume with varying diameters (Balakrishnan and Zrnić 1990). After the investigation of these hydrometeors in separate volumes, the authors conclude that rain's influence on ρ_{hv} is likely caused by the size/shape of the raindrops, while hail and snow's influence on ρ_{hv} are likely caused by physical factors that can lead to highly varying physical features of the hydrometeors. It was also noted that mixtures of precipitation (rain and hail, graupel and hail, or snow and rain) within a volume can lead to similar decreases in $\rho_{hv.}$ These mixtures are commonly found in bright banding features where reflectivity values are high and ρ_{hv} values will be lower than seen in rain (<0.97).

ii. Differential Reflectivity (Z_{DR})

Differential reflectivity (Z_{DR}) is a ratio of the backscatter of energy with horizontal and vertical polarization factors (Seliga and Bringi 1976; Pointin et al. 1988; Crowe et al. 2012). This variable provides insight into the size and shape of hydrometeors within a sample volume. Z_{DR} can be positive or negative in both meteorological and non-meteorological scatterers. Negative Z_{DR} values indicate that hydrometeors within the volume are more vertically oriented (values can reach ~-8 dB; NOAA 2018), while positive values indicate a more horizontal orientation (values can exceed 8 dB; Palmer et al. 2011; NOAA 2018). Although, Z_{DR} values are capped within the WSR-88D network and values 8 dB or larger are not shown. Spherical raindrops yield values near 0.0 dB when located within a region of lower Z_{HH} (values near 0.0 dB may also occur within regions high Z_{HH}, which may indicate the presence of hail; e.g. Balakrishnan and Zrnić 1990; Heinselman and Ryzhkov 2006; Crowe et al. 2012). For example, large hail would

yield a very low positive to slightly negative value because hail tends to tumble as it falls, while typical raindrops yield positive values which increase as the drops increase in size.

Some common applications for Z_{DR} include hail and tornado debris detection, updraft characterization, identification of the rain/snow transition, and for non-meteorological echoes (specifically for biological scatterers and tornado debris). Although Z_{DR} is helpful in identifying non-meteorological echoes when coupled with other variables, ρ_{hv} is a more accurate way to determine these scatterers because of the very low values exhibited (Balakrishnan and Zrnić 1990). Within this paper, the only applications discussed will be hail detection and updraft intensity. Kumjian and Ryzhkov (2008) describe that low Z_{DR} (near zero dB) collocated with high Z_{HH} at the lowest radar elevation scan indicates that large hail is likely to be present and reaching the ground, depending on the base scan altitude of the beam. The authors also discuss that within the melting layer of a supercell, hail will begin to melt and a water torus will form on the outside of the hailstone. This water torus will cause the hailstone to appear as a large raindrop, yielding strongly positive values of Z_{DR}.

d. Dual-Polarization Radar Signatures

i. Z_{DR} Columns

Z_{DR} columns are common polarimetric signatures in a thunderstorm's updraft region (Conway and Zrnić 1993; Kumjian and Ryzhkov 2008). Kumjian and Ryzhkov (2008) investigated Z_{DR} columns, particularly in supercell thunderstorms, and described them as narrow columns with large Z_{DR} values (often >3 dB) that can extend several

kilometers above the environmental freezing level in the storm's updraft, and are generally found within the weak echo region (WER) of the supercell. Generally, these higher values of Z_{DR} indicate the presence of large oblate raindrops being advected vertically through the updraft. They discuss that the Z_{DR} column is associated with a positive temperature perturbation induced by the convective updraft, which is why the Z_{DR} column is considered a proxy for the thunderstorm's updraft. Figure 3 is an example of a Z_{DR} column when looking at both Z_{HH} and Z_{DR} fields. Research conducted by Hubbert et al. (1998) discussed how the Z_{DR} column is generally collocated with the region of the strongest horizontal convergence in a thunderstorm, which is later used as a proxy for the location of the thunderstorm's updraft. At the top of the Z_{DR} column, it is likely that mixed-phase hydrometeors can be found as the liquid hydrometeors lofted through the updraft begin to freeze and serve as hail embryos. The Z_{DR} column's changing height within a storm can be utilized to determine if a convective cell is strengthening or weakening (Hubbert et al. 1998; Kumjian and Ryzhkov 2008; Kumjian et al. 2010). Intensifying and decaying updrafts were measured through observations of the changing heights of the Z_{DR} columns, along with changes in the magnitude of Z_{DR} values within the column; although this method shows less of a correlation with updraft intensification (Kumjian et al. 2010). It was also determined that examination of the Z_{DR} column within multicellular convection can be useful for determining which cells are intensifying and which are decaying. They also presented similar findings regarding the relationship between fluctuations of the Z_{DR} column and the resulting observations of the convective updraft. It was also found that when the updraft began intensifying, the Z_{DR}

column would expand in areal extent, although, there was no noticeable increase in the Z_{DR} values found within.

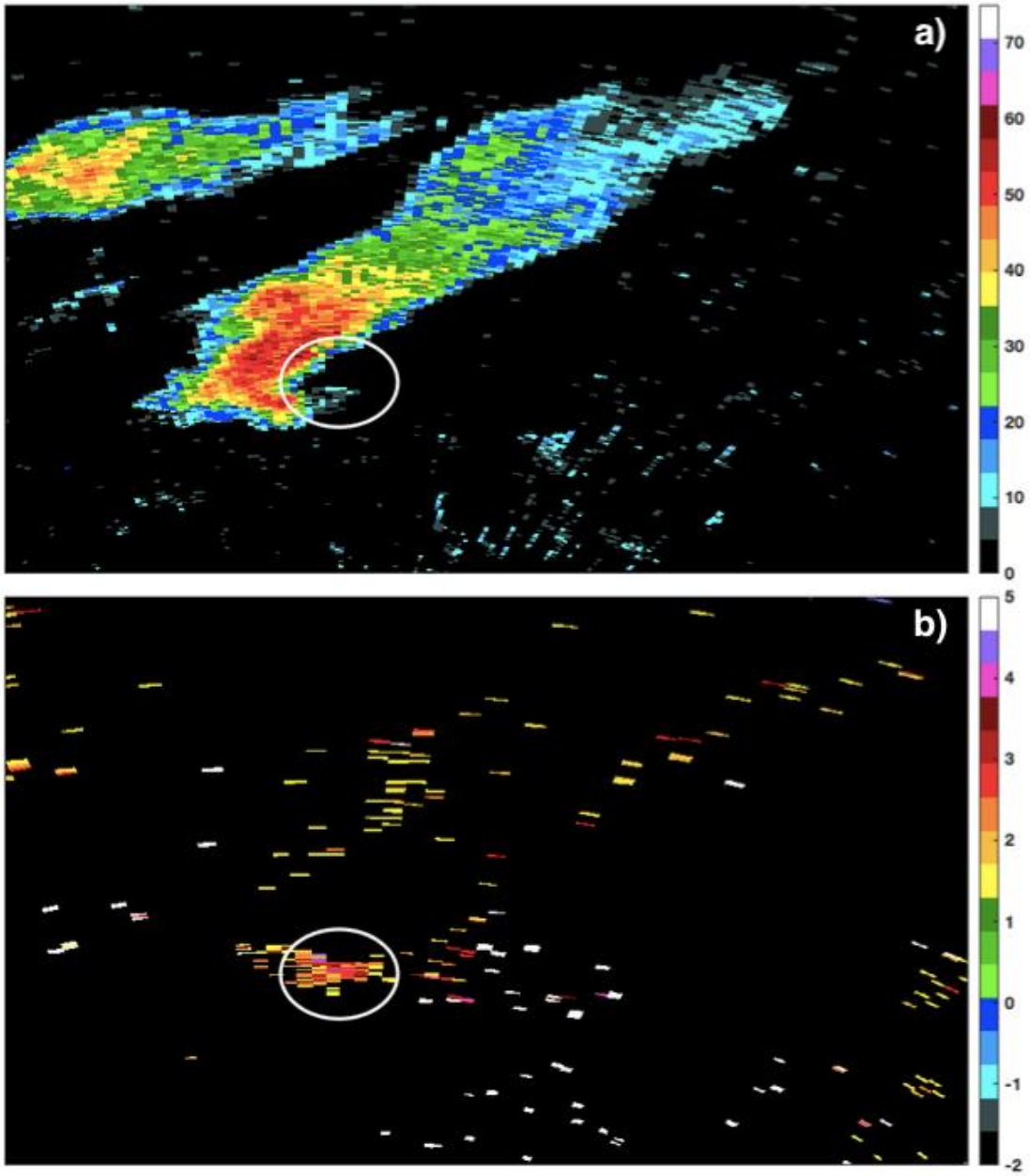

Figure 3. Example of a Z_{DR} column when utilizing radar reflectivity at the base scan (panel a; dBZ) and differential reflectivity at the same location and at a 5.07° (~5 km) elevation angle (panel b; dB). This shows the general region where a Z_{DR} column can be found in the reflectivity field (white circle), along with how it appears in the differential reflectivity field.

Research conducted by Van Den Broeke (2016) investigated the areal extent of the 0.5-dB Z_{DR} column at 1 km above the freezing level, along with the maximum vertical extent of the 1-dB column above the environmental freezing level. When analyzing the maximum vertical extent of the 1-dB column, it was found that supercell thunderstorms within similar environments yielded column heights with similar heights above the freezing level, while storms in different environments yielded statistically different column heights. MUCAPE was found to have a positive correlation with the height of the observed Z_{DR} columns, since higher MUCAPE environments generally support stronger vertical motion within the updraft. Analysis of the 0.5 dB column areal extent generally indicated similar results as the previous analysis, where supercells within similar environments yielded similar areal extents of the observed Z_{DR} columns and were different between differing environments.

Van Den Broeke (2017) investigated polarimetric signatures between supercells, specifically those that were tornadic. Storms that produced significant tornadoes (EF3+) exhibited Z_{DR} columns that were larger in both vertical and areal extent compared to storms that produced relatively weak tornadoes (EF0). It was also concluded that storms that produced significant tornadoes exhibited variable Z_{DR} arc and inferred hail signatures, although the updraft intensity and size were fairly consistent. Through a tornado's lifetime, the Z_{DR} column generally decreased in vertical and areal extent between the genesis of the tornado and the demise.

ii. Low-Level Radar-Inferred Large Hail Signature

The hail core can be inferred through the use of Z_{DR} and Z_{HH} (Heinselman and Ryzhkov 2006). In general, hailstones tend to tumble as they fall through a thunderstorm, which in turn leads to a decrease in Z_{DR} to around 0.0 dB since the hailstone would appear nearly spherical to the radar. Through observations of hail-producing thunderstorms, Balakrishnan and Zrnić (1990) found values that can indicate large hail falling out of the storm. They found that storms producing large hail generally exhibited negative Z_{DR} values in the low and midlevels of the thunderstorms, generally <-0.5 dB, while large and dry hail can also be observed yielding Z_{DR} values between 0.0 and -0.5 dB. Several investigations (e.g., Balakrishnan and Zrnić 1990; Heinselman and Ryzhkov 2006; Kumjian and Ryzhkov 2008) have utilized ρ_{hv} data to better distinguish rain, hail, and non-meteorological echoes in supercells. These studies have indicated that small decreases in the ρ_{hv} from the normal value for rain, 0.98, can indicate the presence of smaller hail that is likely mixed with raindrops, while with increasing hail size and for hail becoming drier the ρ_{hv} values can drop to 0.90 or less.

Typically, using S-band radar, a core of large hail within a supercell can be observed as a region of low Z_{DR} (around 0.0 dB) surrounded by a region of larger Z_{DR} values at the lowest elevation scan. This indicates that larger hail is characterized by low Z_{DR} due to its tumbling nature, with the surrounding area dominated by larger raindrops or water-soaked hail, shown by the larger Z_{DR} values (Kumjian and Ryzhkov 2008). If this signature is found within a storm at the lowest-elevation radar scan, it is a good

indication that hail is reaching the ground. Figure 4 is an example of a supercell which shows the Z_{DR}-inferred hail core at the base radar scan. They also found that in a sample of tornadic supercell cases, the majority of the supercells exhibited a hail core more often while there was a tornado, compared to the times before and after the tornado. It was also found that in a sample of nontornadic cases, most volume scans exhibited an inferred hail core.

Research conducted by Van Den Broeke (2016) found that the low-level inferred hail core was generally located downshear from the supercell's mesocyclone. This investigation specifically focused on the areal extent of the inferred hail core between similar and different environments, while also analyzing the variability of the hail core at a scanning altitude of <1 km ARL. Van Den Broeke generally found that supercells may exhibit a cyclic hail core, where some low-level scans will show a large core and others may show little to no hail core. Generally, storms in similar environments contained similar areal extents of inferred hail, while storms in different environments varied, although, not as significantly as the other polarimetric signatures investigated. The height of the level of free convection (LFC) was found to be the best-correlated environmental variable with the hail core's areal extent. Storms that formed in environments with higher LFCs generally were associated with larger inferred hail cores, likely because an elevated LFC would indicate an updraft that is at a higher altitude and would be relatively colder than LFCs that are closer to the surface. Temporal variability of the hail core size was found to vary widely between tornadic and nontornadic storms, with increasing variability in higher MLCAPE environments (Van Den Broeke 2016). While variability

generally increased with increasing MLCAPE, it decreased in environments with increasing SREH (Van Den Broeke 2016).

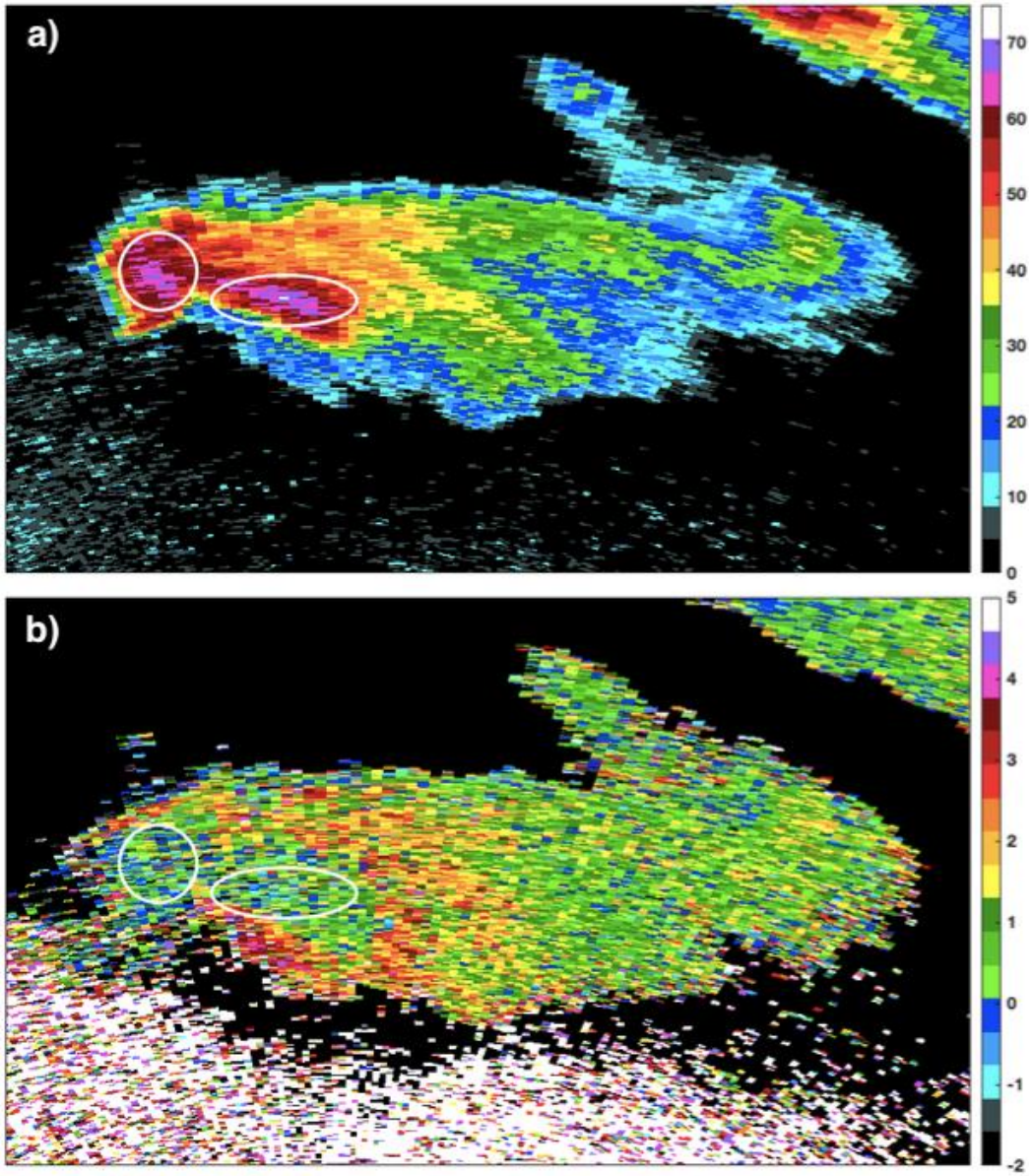

Figure 4. Example of a low-level Z_{DR} inferred hail core utilizing radar reflectivity (panel a; dBZ) and differential reflectivity (panel b; dB). White annotations show the general region where an inferred hail core can be found in the reflectivity field, along with how it appears in the differential reflectivity field.

iii. Z_{DR} Arcs

Z_{DR} arcs are common features within supercell thunderstorms. They are characterized as an area of enhanced Z_{DR} values along the forward flank of a supercell, generally along the sharp reflectivity gradient in that region (Kumjian and Ryzhkov 2008). Figure 5 is an example of the Z_{DR} arc found in a supercell at the base scan. These features are found in a relatively shallow layer, about 1-2 km above earth's surface. Z_{DR} values can be relatively high within the Z_{DR} arc, with values commonly reaching 4-5 dB (Kumjian and Ryzhkov 2008). These high values indicate scatter dominated by relatively large, oblate raindrops. The presence of these large drops is due to size sorting. Size sorting occurs as a consequence of a veering wind profile, which acts to advect the smaller raindrops out of this region due to their lower terminal velocities, compared to larger raindrops which are not as easily advected and have higher terminal velocities. Specifically, SREH is a key factor to consider when observing storms for Z_{DR} arcs. Since supercell thunderstorms need SREH to induce midlevel rotation because of the necessary ingestion of streamwise vorticity, Kumjian and Ryzhkov (2008) suggest that there is likely a relationship between the SREH and Z_{DR} arcs. Kumjian and Ryzhkov (2009) found a positive correlation between SREH and the magnitude of Z_{DR} values within the arc. Later research conducted by Dawson et al. (2015) describe that the correlation found by Kumjian and Ryzhkov (2009) is more likely a correlation between the SREH and the storm-relative mean winds. Dawson et al. (2015) found that the magnitude of the Z_{DR} arc has a higher correlation with the storm-relative mean wind vector than was found with SREH or shear. They also described that Z_{DR} arcs are prominent in both environments that have higher SREH and

shear, along with environments with little to no SREH and shear. Some nonsupercellular thunderstorms may exhibit an arc-like feature, which is likely caused by a thunderstorm that is ingesting more SREH, possibly leading to midlevel rotation and supercellular characteristics (Kumjian and Ryzhkov 2008).

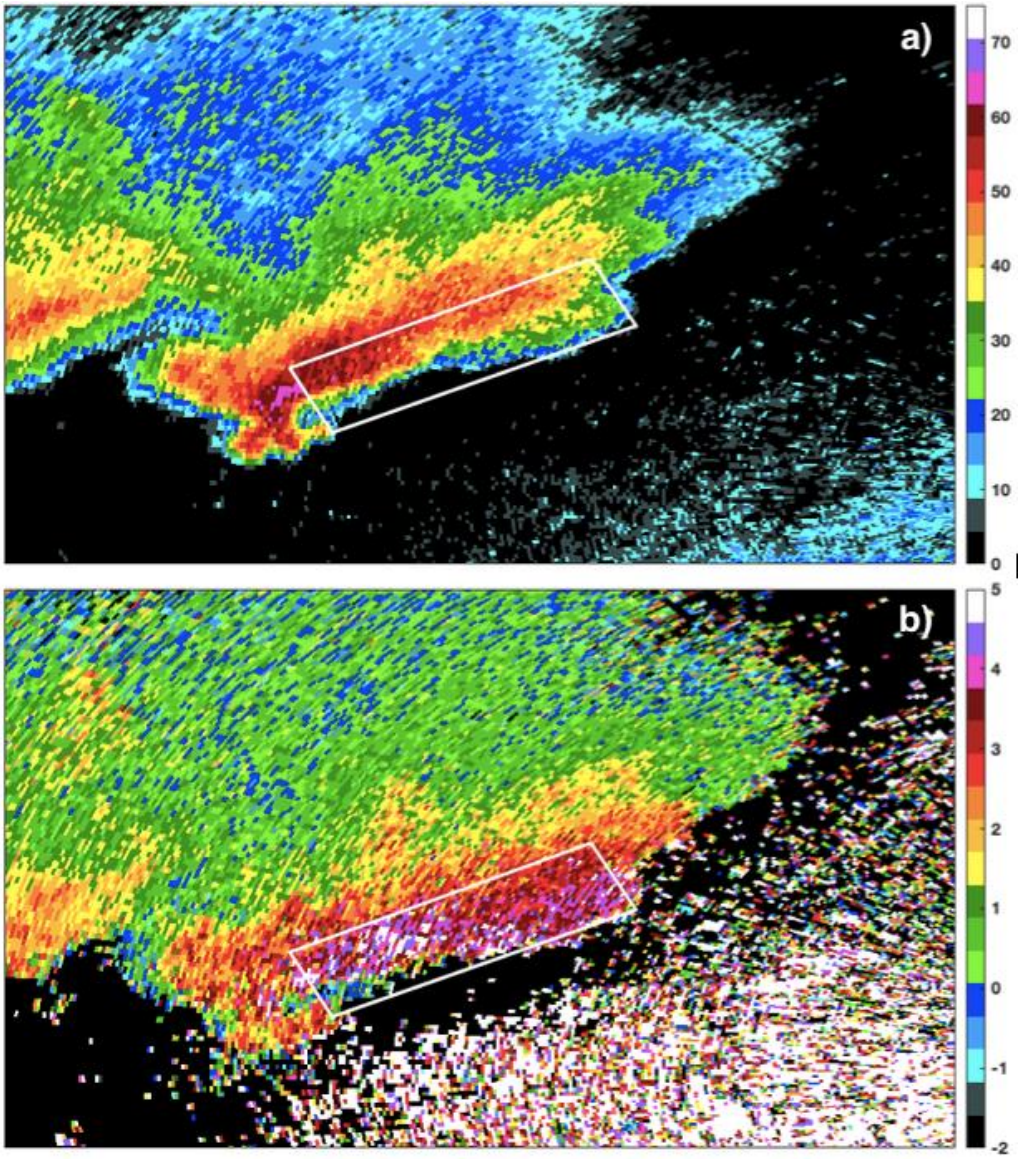

Figure 5. Example of a Z_{DR} arc utilizing radar reflectivity (panel a; dBZ) and differential reflectivity (panel b; dB). This shows the general region where a Z_{DR} arc can be found in the reflectivity field, along with how it appears in the differential reflectivity field.

Later research conducted by Palmer et al. (2011) described several polarimetric variables and signatures during a tornado outbreak on 10 May 2010. The Z_{DR} arc had similar characteristics to those observed in past research, where much higher values of Z_{DR} were observed (>8 dB). They observed the evolution of the Z_{DR} arc and investigated signatures that may be commonly observed in association with tornado-producing supercells. They found that closer to the updraft region, the Z_{DR} arc was not as defined, while farther from the mesocyclone along the forward flank of the supercell, a more solid Z_{DR} arcing feature was observed, consistent with past observations. The supercell observed was cyclic in nature and exhibited a Z_{DR} arc that was initially well defined and then began to deteriorate. Then, the arc quickly reorganized into a well-defined Z_{DR} arc. Similar temporal variability of the arc was noted in the literature prior to this investigation (Kumjian et al. 2010).

More recent research conducted by Van Den Broeke (2016) investigated characteristics of the Z_{DR} arc between supercell thunderstorms in similar and different environments (where the arcs were observed <1 km ARL), such as Z_{DR} arc width (defined by $Z_{DR} \geq 2$ dB), areal extent (area of $Z_{DR} \geq 3.5$ dB), and mean pixel values (all values within the arc ≥ 0 dB). The 1-3 km layer shear within each supercell storm was used as a base comparison with Z_{DR} arc characteristics since this is the layer in which the Z_{DR} arc can be found, along with this layer being the main region in which the size sorting is observed. Although this layer was utilized, different layers may be used in other research depending on the storm structure. Van Den Broeke found that storms within similar environments yielded similar Z_{DR} arc widths, on average, while storms with larger

1-3 km shear also yielded wider arcing features. It was also found that storms within environments with drier midlevels yielded wider Z_{DR} arcs, likely caused by precipitation forming higher within the storm and needing to fall farther to reach the base scan level, leading to a longer time for size sorting to occur. It was also found that although storms within similar environments yielded relatively similar areal extents of the 3.5 dB Z_{DR} arc, the correlation within similar environments was not as high as the other polarimetric comparisons (Z_{DR} columns and Z_{DR}-inferred hail cores) examined in this study. It was found that supercells exhibited similar arcing signatures within lower MUCAPE environments, while the areal extent of the arcs varied widely within increasing MUCAPE environments.

3. Data and Methodology

a. Data

Warm-based supercells were defined as storms that formed in an environment with cloud base temperatures 15 ℃ or warmer, while cold-based supercells were those with cloud base temperatures 5 ℃ or cooler. These cold- and warm-based environments were discussed in research conducted by Van Den Broeke et al. (2008), where these thresholds were chosen due to the general differences in locations where these storms form. The MLLCL (for surface-based supercells) and the mixed-layer convective condensation level (MLCCL; for elevated supercells) were used as proxies for cloud base, sampled at the analysis time nearest the center point of the analysis period, which will be discussed more in the case selection section. Along with the cloud base temperature criteria, each supercell case also had to be relatively isolated from other convection, that way the polarimetric signatures are relatively well resolved without other convection altering their orientations. Supercell cases were found by utilizing the Storm Prediction Center (SPC) storm report archive. While searching through these archives, the goal was to find linear tracks of storm reports (wind, hail, or tornadoes). Once a potential case was found through the archive, radar data were utilized to verify if the storm that produced the reports was a supercell. Specific characteristics used to identify a supercell will be discussed further in the case selection section. If the storm was identified as a supercell, the environment within the inflow region of the supercell was estimated using numerical model output. Velocity data were utilized to determine where the inflow region of the supercell was, specifically looking for where the motion of the targets was towards the

supercell, generally located along the forward flank of the supercell. Once the inflow region was identified, maps that show available ASOS stations were used to determine which site would lie closest to the supercell and within the inflow region of the storm. BUFKIT (NOAA 2019) was used to generate model soundings based on data gathered from the Rapid Refresh (RAP) and Rapid Update Cycle (RUC) sounding archive (Iowa State University 2020), which were determined to be most representative of the inflow region of the supercell based on methods previously discussed. A representative sounding from each storm (gathered from the RAP and RUC sounding archive) was run through BUFKIT to estimate the cloud base temperature of each storm, along with gathering several other environmental characteristics. Radar data were analyzed through NOAA's Weather and Climate Toolkit (WCT; NCEI 2019) for the WSR-88D radar site that was closest to the supercell. WCT was where radar data were also exported from to later interpret through GIS software. QGIS (2019) was utilized to display and filter the radar data to later statistical analyze.

b. Cases

Supercell thunderstorm events were selected from the entire CONUS region. Since the goal of this project was to analyze polarimetric radar signatures, radar data from 2012 through 2019 were investigated as the radar network went through the transition to dual-polarization between 2012 and 2013. A total of 30 supercell cases were found and investigated, with 15 being warm-based and 15 cold-based supercells (Table 1). Each of these supercell thunderstorms had to be located within 75 km of a radar site, and had to be supercellular in nature for at least 45 minutes, by exhibiting a persistent mesocyclone

in the mid-level velocity data through the entire supercell's observational period. A distance of 75 km was required because low-level radar features in the supercells are typically well-defined in radar data at ~1 km AGL, which yields a threshold distance of about 75 km assuming standard beam propagation. This distance threshold was utilized for proper analysis of the inferred Z_{DR} hail cores and the Z_{DR} arcs. This distance threshold was determined based on the equation used to determine the height of the radar beam in a standard atmosphere (Equation 1). The 4/3 earth assumption was utilized to determine the effective radius of the earth, R_e'. The beam height was determined by the distance from the radar, s, at a constant elevation angle of 0.5°, ∅, and with a radar height of 30 m, h_0 (Rinehart 2010).

$$h_s = \frac{s^2}{2R_e'} + \Phi_0 * s + h_0 \qquad (1)$$

The goal of this project was to investigate each supercell storm for at least 45 minutes, which was, on average, about 11 time steps or more, depending on which scanning strategy was in use by the radar. Several of the cases used a supplemental adaptive intra-volume low-level scan (SAILS) strategy, which assists meteorologists in getting frequent low-level radar scans during rapidly evolving situations (Chrisman 2014).

As long as the storm met the criteria listed above and met the time requirement, it was included. Some storms exhibited data quality errors during some of the time steps, so only those time steps were removed. Data quality errors generally arose when the storm would propagate very close to or across the radar site, where necessary data were missing due to the storm's proximity to the cone of silence. Some locations also had objects that

obscured the data such as wind farms or mountains, and time steps were neglected if these features were present.

The geographical distribution of the 30 supercell cases investigated is depicted in Figure 6. Most of the warm-based supercells were observed within the central and eastern United States, while the cold-based supercells were generally observed in the central and western United States, usually at locations with higher altitude.

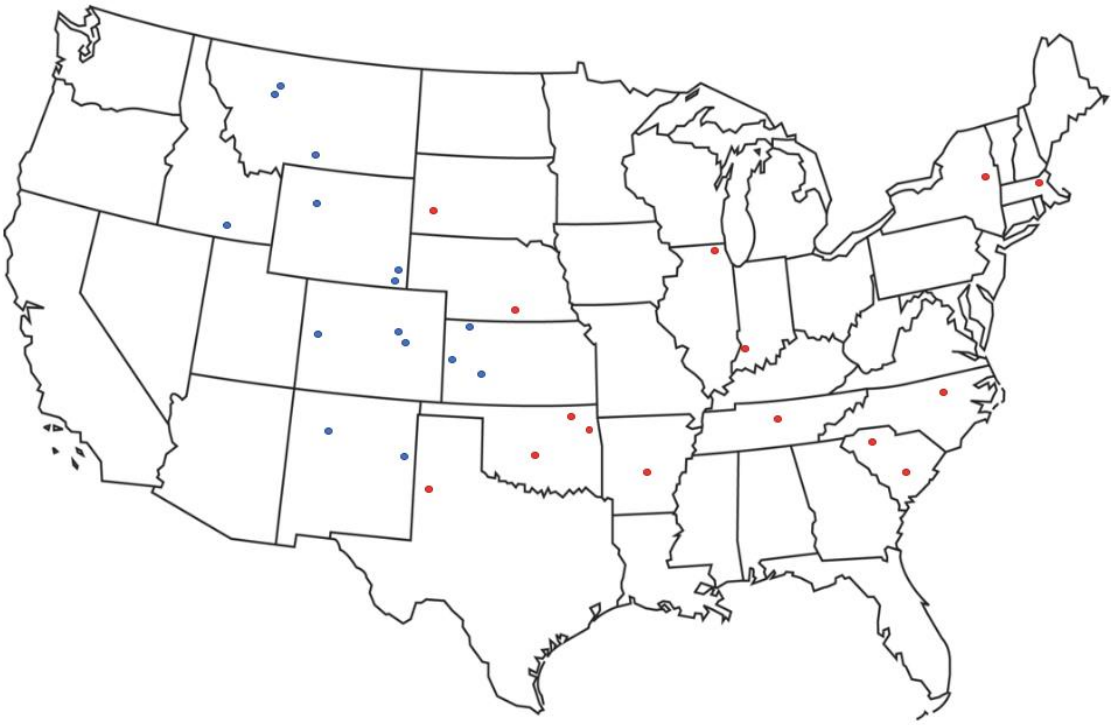

Figure 6. Geographic distribution of supercell cases. The red circles indicate the locations of the warm-based supercells, while the blue circles indicate the locations of the cold-based supercells.

Table 1. All supercell cases analyzed for this project with the respective radar sites, dates, and observation times. "*" indicates if there were some data quality errors during the observational period, along with the number of neglected time steps.

Location	**Date**	**Time (UTC)**
	Warm	
KOHX	4-27-2012	2332-0018
KINX	5-20-2013	2029-2117
KTLX	5-30-2013	1928-2032
KINX	5-31-2013	0003-0051
KGSP	6-2-2013	2018-2105
KCAE	6-4-2013	1854-1942
KLOT	6-12-2013	2143-2230
KRAX	6-18-2013	2154-2240
KLBB	6-19-2013	2207-2259
KVWX	11-17-2013	1921-2007
KLZK	12-21-2013	2341-0027
KENX	7-3-2014	2008-2101
KBOX	7-7-2014	2103-2155
KUDX	6-8-2018	2139-2232
KUEX	6-30-2018	2046-2147
	Cold	
KGLD	3-29-2013	2312-2357
KGLD	3-30-2013	0055-0146
KDDC	5-7-2013	2324-0011
KBLX	6-19-2013	2146-2233
KFDX	6-21-2013	2246-2342
KTFX*(5)	5-4-2014	2115-2226
KGJX	5-22-2015	1814-1905
KABX	5-15-2016	1930-2030
KSFX	5-20-2018	1917-2003
KFTG	5-21-2018	2229-2336
KCYS	5-6-2019	2150-2238
KTFX	6-14-2019	2013-2134
KRIW	6-15-2019	2039-2205
KFTG	9-10-2019	2307-2355
KCYS	9-20-2019	2036-2123

c. Z_{DR} Calibration

Anomalously high or low Z_{DR} values are often observed within convection, often due to resonance effects and radar system drift out of calibration (Picca and Ryzhkov 2012). A scatterer-based Z_{DR} calibration method designed by Picca and Ryzhkov (2012) was applied to all Z_{DR} data utilized, which helped to correct any errors that may occur within the radar system that would also lead to anomalously high or low Z_{DR} values. These errors are caused by calibration drift within the radar system. This calibration method was applied to regions of inferred pristine ice crystal aggregates within the anvils of supercells about 1.5 km above the melting layer, where there are Z_{HH} returns of 20-35 dBZ and the ρ_{hv} returns are larger than 0.97. From this area, the associated Z_{DR} values were extracted. The average of all the Z_{DR} pixel values that coincide with these Z_{HH} and ρ_{hv} threshold values were compared to the Z_{DR} value that represents pristine ice crystals. Since pristine ice crystals have considerable variation in Z_{DR} values based on their structure, 0.15 dB will be the typical value used, where it is assumed that dry snow aggregates are being observed. The average Z_{DR} value within the extracted region was then subtracted from 0.15 dB, yielding a calibration factor which was added to all Z_{DR} data used in the following analyses.

Resonance effects can also occur due to the presence of hail or raindrops that are larger than the wavelength used by the radar, which can lead to worse effects of attenuation or differential attenuation, especially with the presence of large hail (Kumjian and Ryzhkov 2012). Since the goal of this project is to investigate polarimetric signatures within supercell thunderstorms where hail and large raindrops are common,

resonance effects must be considered when utilizing Z_{DR} data (Picca and Ryzhkov 2012). Resonance effects were monitored to ensure that they did not impede any signatures investigated.

d. Environmental Characteristics

Environmental data gathered from the RAP and RUC sounding archive (Iowa State University 2020) provided information regarding atmospheric conditions in each supercell environment. Soundings utilized were representative of the conditions within the inflow region of the supercells, which were used to describe the near-storm environment. Environmental variables gathered include cloud base height (MLLCL or MLCCL height), MUCAPE, effective storm relative helicity (ESRH), effective bulk shear (ESHEAR), 3-6 km relative humidity (RH), 0 ℃ level, cloud base temperatures (MLLCL or MLCCL temperatures), 0-1 km SRH, 0-1 and 0-6 km shear, and 0-3 km vorticity generation parameter (VGP; Rasmussen and Blanchard 1998). The soundings were gathered for the analysis time nearest to the midpoint of the observational period. The soundings were input to BUFKIT, which allowed the calculation of numerous environmental characteristics. A statistical analysis could then be completed to compare the subsets. A Wilcoxon-Mann-Whitney (WMW; Wilks 2006) test was run with the assumption that the two sets of supercells (warm- and cold-based) will exhibit distinct environmental characteristics. This statistical analysis was chosen for this investigation because this is a nonparametric statistical test which can be used for a non-Gaussian distribution, which compares the two distributions and tests for the statistical significance of the differences between the two samples. For the purposes of this project the

hypothesis used for this test was that the two sets of data come from the same larger subset of storms. Once the data were run, the WMW test provided *p*-values which provided insight into the nature of the two samples, providing evidence for whether the supercells could be considered part of the same population or if they were likely from a separate population. Significant levels for this analysis were set to α=0.05. *P*-values that were less than 0.05 indicated that the null hypothesis (H_o) was rejected and that the two sets of values were not taken from a similar population, while those with p>0.05 indicated that they were drawn from similar populations.

e. Z_{DR} Columns

The Z_{DR} column height and areal extent were analyzed using WCT (NCEI 2019) and GIS (QGIS 2019) software. The height of the Z_{DR} column was defined as the height relative to the radar. The criteria used to identify the Z_{DR} column were observations of a localized area within the Z_{DR} field that has several pixels collocated with Z_{DR} values larger than 1 dB, along with the column having vertical continuity within the storm as radar elevation angle increased. Previous studies have investigated the general location of the Z_{DR} column and results indicated that the column was consistently found on the fringe of the BWER and within the inflow region, generally along the main updraft of the storm (Kumjian and Ryzhkov 2008). A BWER and WER are not required for there to be a Z_{DR} column, as these can be found within storms that do not exhibit either. The height of the environmental 0 ℃ level was then subtracted from the height of the Z_{DR} column top, providing the depth of the Z_{DR} column. Cases that showed a negative height above 0 ℃, indicating a Z_{DR} column height lower than the 0 ℃ level, were recorded to be 0 km above

the melting layer (e.g., no Z_{DR} column existed). The mean Z_{DR} column height above the 0 °C level was also compared to the MUCAPE values corresponding to the environments that the supercells occurred in. Increasing environmental instability should lead to storms that exhibit stronger updrafts, which in turn should yield a Z_{DR} column that extends higher above the 0 °C level.

The areal extent of the Z_{DR} column was also investigated. Data were imported into GIS, aiding in the calculation of the areal extent of the Z_{DR} column. The areal extent of the 0.5 dB column was calculated for each time step and averaged over the observational period. This average areal extent was then compared between warm- and cold-based supercells, along with the 90th percentile of the pixel values within the calculated area. Percentile values for time steps where the supercells did not exhibit a column were recorded as "NA."

f. Low-Level Radar-Inferred Large Hail Signature

The low-level radar-inferred large hail signature was determined to be the region in the core of the storm and at the lowest elevation angle where Z_{DR} values were between -0.5 and 1.0 dB and Z_{HH} values were at least 55 dBZ, following prior studies (e.g., Heinselman and Ryzhkov 2006; Kumjian and Ryzhkov 2008; Dawson et al. 2014; Van Den Broeke 2016). Each calculation for the hail core utilized constant altitude plan position indicator (CAPPI) data at 1 km ARL, to sample at a consistent level within the observed storms. Each case needed to be within the spatial limits for at least 45 minutes of the supercell's lifetime, while only 3 full radar scans were required to perform an analysis. The areal extent (km^2) of the hail core was averaged over all time steps for each

case. The coefficient of variation (COV) was calculated for all of the time steps associated with each case, providing information regarding how much the hail core changes in the observed time frame. The COV is calculated by taking the standard deviation of the areal extent of the hail core divided by the average areal extent over the complete time series for a given storm. The COV was utilized to provide a quantitative value that represents the amount of variability between the time steps for a given case, since supercell thunderstorms are known to have cyclic hail cores. These methods are similar to those used in past research (Van Den Broeke 2016). This metric will provide information regarding which environment (cold- or warm-based environments) was associated with a more variable hail core.

Once the average areal extent of the hail core was calculated for each case, the 35 dBZ storm areal extent was determined using similar methods. For each case, the calculated areal extent of the hail core was normalized to the 35 dBZ core for each time step, providing a standard metric to compare the average inferred hail core size between supercells within the same and differing environments. Normalizing the hail core size to the 35 dBZ core was completed by dividing the areal extent of the inferred hail core by the areal extent of the 35 dBZ core for each time step. After this value was calculated for each time step, the average value was calculated for each case. These average normalization values indicated what percentage of the low-level reflectivity core was typically inferred hail.

g. Z_{DR} Arc

The Z_{DR} arc was identified at the lowest elevation angle along the forward flank of the supercells. The values of Z_{DR} within the Z_{DR} arc can exceed 4-5 dB (Kumjian and Ryzhkov 2008). Therefore, the Z_{DR} values were filtered to show all values of at least 3.5 dB for the warm-based supercell cases, as was used in a similar investigation by Van Den Broeke (2016). Investigations of cold-based storms with the 3.5 dB threshold were initially completed, although, they lead to most cases without a Z_{DR} arc identified. Therefore, a threshold of 2.5 dB was used as a filter for cold-based storms due to the data limitations and possible microphysical differences between these types of storms. Microphysical differences can be present since the cloud bases are much higher, on average, in cold-based environments compared to the warm-based environments. Higher cloud bases bring the cloud base closer to the environmental 0.0°C level. Much of the arc in cold-based storms may originate from water-coated hail, exhibiting larger Z_{DR} values. Therefore, cold-based storms with a smaller hail core may not exhibit a noticeable Z_{DR} arc. An average Z_{DR} arc areal extent (km^2) was calculated for each storm. The Z_{DR} arc was identified based on the continuity observed between the pixels in the forward flank. If more "gaps" became evident in the Z_{DR} data (indicating values smaller than the thresholds), these data would not be considered as part of the Z_{DR} arc (Figure 7). These arcing features were manually selected instead of using computer algorithms because this was determined to be the most accurate approach. Along with the areal extent being calculated, the 90^{th} percentile of the Z_{DR} values were also determined for each arc.

Percentiles for the time steps where the supercells didn't exhibit an arcing feature were considered as "NA."

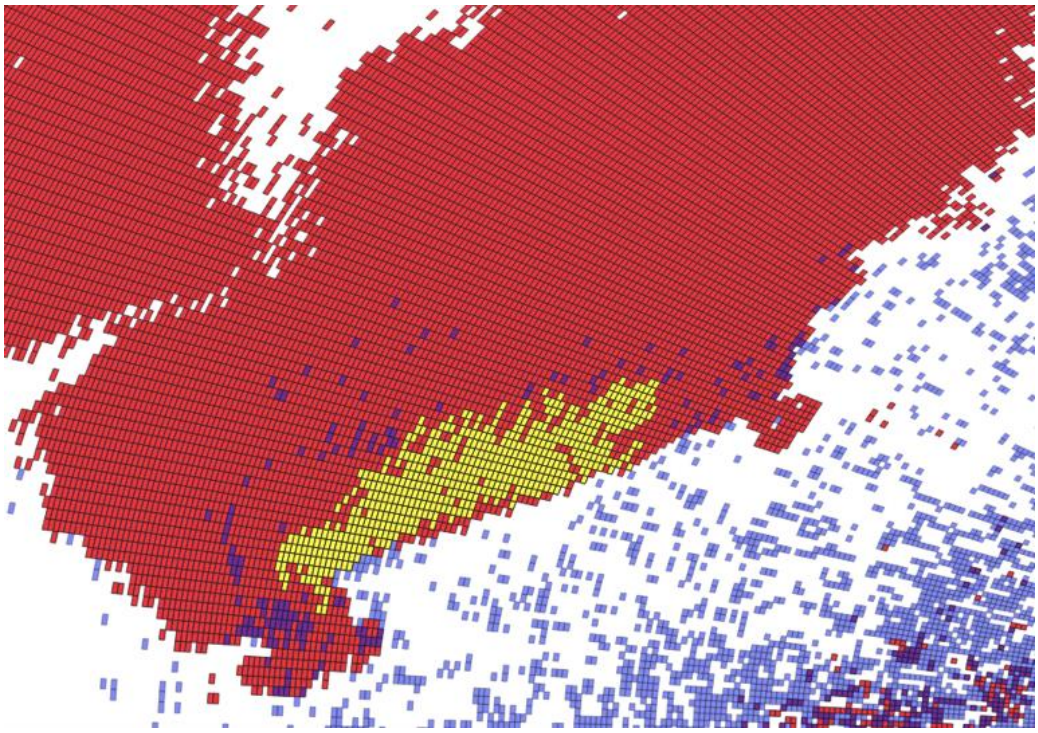

Figure 7. An example showing the region in which the Z_{DR} arc was manually selected, based on the continuity of the pixels found within the forward flank of the supercell. The red pixels indicate the regions that exhibit Z_{HH} > 15 dBZ, while the blue pixels indicate the regions that exhibit Z_{DR}>3.5 dB. The yellow region is the area selected as the Z_{DR} arc.

4. Results

a) Environmental Variability

Warm-based supercell cases were found to have cloud base heights that were generally around 1 km or less, with the highest cloud base at 1.20 km. Cold-based supercells generally exhibit cloud base heights above 1 km (only one case <1 km), and the highest cloud base is at 3.89 km. Between both supercell types, about 80% of the cold-based supercells exhibit cloud base heights greater than all warm-based cases, 12 out of the 15 cases (Figure 8b). A comparison between median values shows a large significant difference (p=4.68E-05), where warm-based supercells exhibit a median cloud base height of 0.49 km, while the median for the cold-based storms is at 2.38 km. The warm-based supercells are generally found in significantly different environments, with cloud base temperatures between 17 °C and 23 °C and the cloud base temperature range for cold-based storms is -5 °C to 5 °C (Figures 8a). The height of the 0 °C level provides insight about when melting of hail might begin. With warmer profiles observed in the warm-based cases, higher 0 °C levels are expected. Warm-based supercells exhibit environmental 0 °C levels that are all >3 km above the surface, with the highest at 4.10 km. Cold-based storms have thermodynamic profiles that are much cooler than the warm-based cases, have much higher cloud base heights, and cloud bases that are already relatively close to 0 °C (if not below). Since these environments are much cooler than those of the warm-based cases, 0 °C levels for the cold-based cases range between 1.31 and 3.61 km. While the cold-based supercells exhibit 0 °C levels that are relatively lower in the atmosphere, ~87% of the warm-based storms exhibit 0 °C levels that are higher

than all of the cold-based supercells (Figure 8c). The WMW test for the 0 °C levels also yielded statistically significant differences between the two types of supercell environments (Table 2).

Table 2. The mean, standard deviation, and *p*-value for each set of supercells

	Mean		Standard Deviation		
Variables	**Warm**	**Cold**	**Warm**	**Cold**	***P*-Value**
Cloud Base Height	0.53	2.30	0.36	0.83	4.68E-05
0 ℃ Level	3.82	2.45	0.27	0.56	6.10E-06
MUCAPE	2145.53	503.00	1288.17	308.01	7.12E-05
ESRH	176.07	54.47	137.17	42.31	1.19E-03
ESHEAR	33.47	21.07	13.31	9.41	4.15E-03
RH: 3-6 km	55.26	55.60	24.10	17.89	9.30E-01
Cloud Base Temperature	20.49	0.90	1.73	3.41	3.30E-06
0-1 km SRH	134.87	43.07	124.38	36.33	2.63E-03
0-1 km Shear	12.00	6.07	6.50	2.74	3.09E-03
0-6 km Shear	39.00	29.20	11.00	9.92	5.00E-02
0-3 km VGP	0.34	0.17	0.088	0.054	1.25E-06
ML Mixing Ratio	15.00	5.70	1.66	1.14	3.38E-06

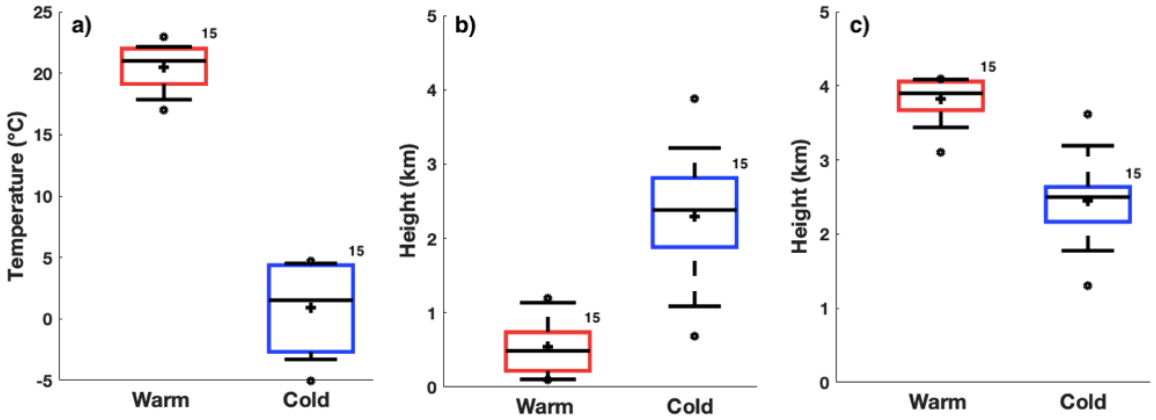

Figure 8. A comparison of a) cloud base temperatures, b) cloud base heights, and c) 0 °C level. Within each boxplot, the first quartile indicates the 25th percentile, the third quartile indicates the 75th percentile, the whiskers indicate the 9th and 91st percentile, the bar within the box indicates the median, the mean value is represented by the cross, and the circles indicate outliers. The numbers next to the boxplots indicate the number of cases that contribute to the spread.

Environmental winds play a crucial role in the organization and maintenance of convection, including supercell thunderstorms. The 0-1 km shear, 0-1 km SRH, 0-6 km shear, ESHEAR, and ESRH were investigated to gain an understanding of the wind profiles within the environments of cold- and warm-based supercells. The low-level (0-1 km) wind shear and SRH are similar between the two environments. Generally, warm-based storms occur with stronger shear in the low levels, with the highest 0-1 km shear at 27 m s^{-1}, where the highest 0-1 km shear observed in the cold-based cases is 11 m s^{-1}. Although the difference between these maxima is large, the distribution of the data shows environments that are not as different. Only ~53% of the warm-based supercells are found in environments with higher shear than the cold-based supercells, where there is ~47% overlap (where the values fall within the 9%-91% values of both cold- and warm-based supercell environments) between the two datasets (Figure 9a). Although there is a large overlap between the two sets of cases, there is a large enough difference between the medians in each data set for this difference to be statistically significant (Table 2). Similar results are found for the low-level SRH, as the highest SRH in the warm-based cases is 482 m^2 s^{-2}, and the highest in the cold-based cases is 126 m^2 s^{-2}. Although these two maxima are very different, there is a 47% overlap between the two datasets (Figure 9d). The cold-based supercells generally are associated with SRH values on the low end of the spread of the SRH for the warm-based cases, where 14 out of the 15 cold-based cases yielded SRH values lower than the median value in the warm-based environments and thus yielded a low WMW *p*-value (Table 2). Deep layer (0-6 km) shear slightly differs between the cold- and warm-based environments, with a median value for the

warm-based supercells of 39 m s^{-1} and the median value in the cold-based supercell cases of 25 m s^{-1}. Although the median between the two data sets show a slight difference, about 93% of the data from the two data sets overlap. A 93% overlap indicates that there are no large differences in the deep-layer shear between the two environments, with a *p*-value of 0.05, indicating statistical similarities (Table 2). Similar results were found for ESHEAR and ESRH. About 73% of the ESRH data and ~67% of the ESHEAR data overlap between the two environments (Figure 9c, d). Although, the calculated *p*-values for ESRH and ESHEAR indicates a statistically significant difference.

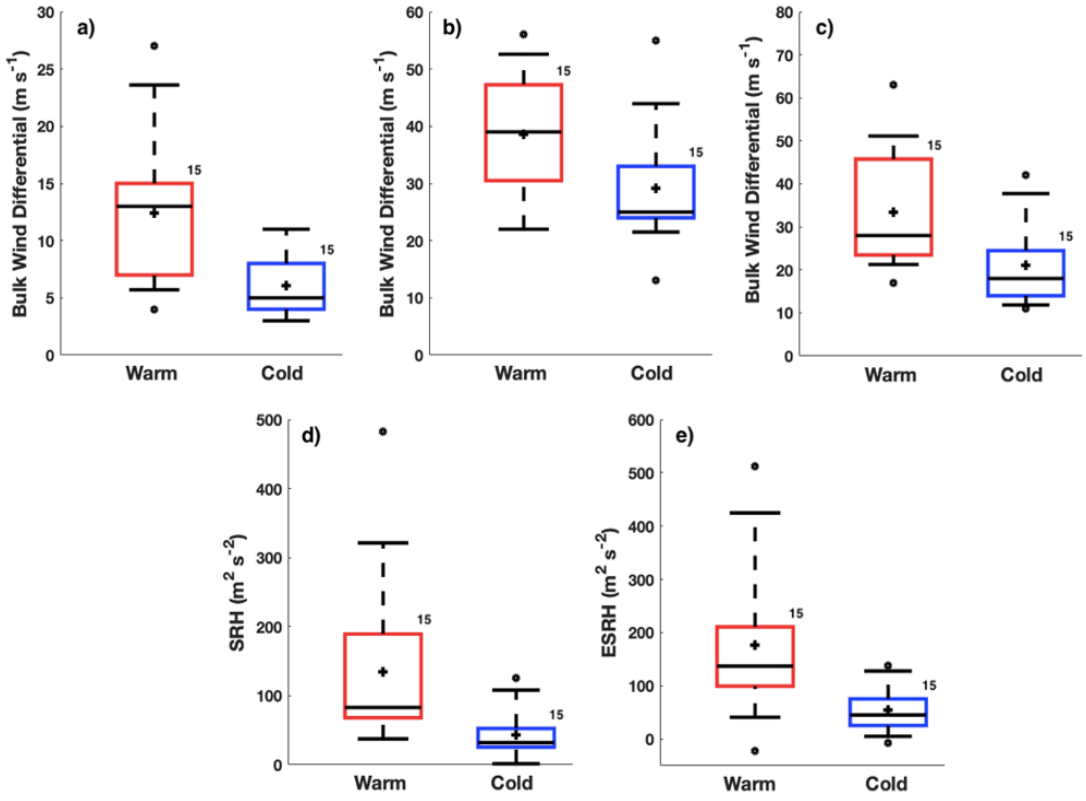

Figure 9. As in Figure 8, except for a comparison of a) 0-1 km shear, b) 0-6 km shear, c) ESHEAR, d) 0-1 km SRH, and e) ESRH.

MUCAPE was assessed as a measure of instability within the two sets of environments and may be related to potential strength of supercell updrafts. The warm-based supercells are all found in environments with MUCAPE >1000 J kg^{-1}, with the highest MUCAPE at 4951 J kg^{-1}. While the warm-based storms are generally found in higher MUCAPE environments, only two of the cold-based supercells are found in an environment with MUCAPE >1000 J kg^{-1}, with the highest MUCAPE value of 1093 J kg^{-1} in the cold-based supercells (Figure 10a). The 0-3 km VGP, which provides information regarding the rate of stretching and tilting of the horizontal vorticity field near the updraft (Rasmussen and Blanchard 1998), is generally higher in warm-based supercell environments. About 53% of the warm-based storms have higher VGP than all the cold-based cases (Figure 10b). Warm-based supercells are generally associated with higher VGP values because VGP is strongly a function of the environmental CAPE. Therefore, VGP should be significantly higher in high CAPE environments, such as the warm-based environments. A pressure-weighted average relative humidity (RH) was calculated for each storm to assess the amount of midlevel moisture between the two sets of environments. Analyzing the moisture content can provide useful information about microphysical processes, including how hydrometeors may change phase or size within the midlevels if environmental air is entrained. Results indicate that the midlevel moisture content within each set of environments is variable with no significantly (p=0.967) large differences between environments (Table 2). Approximately 80% of the warm-based storms had midlevel RH values that overlap those observed in the cold-based environments (Figure 10c). Finally, the 100 mb ML mixing ratio was calculated for each

case across environments to get an idea regarding how dry or moist the near surface layer is in each type of supercell environment. The mixing ratio is statistically different across environments (see Table 2), where the cold-based supercells are generally found in environments with relatively drier (~5-7 g kg^{-1}) near-surface air and the near surface air in the warm-based supercells is moister (~15 g kg^{-1}). The drier conditions observed in these cold-based supercell environments is likely a large factor leading to the higher cloud bases that are observed, where moist near-surface air wouldn't need to lift high to reach saturation, as seen in the warm-based supercell environments.

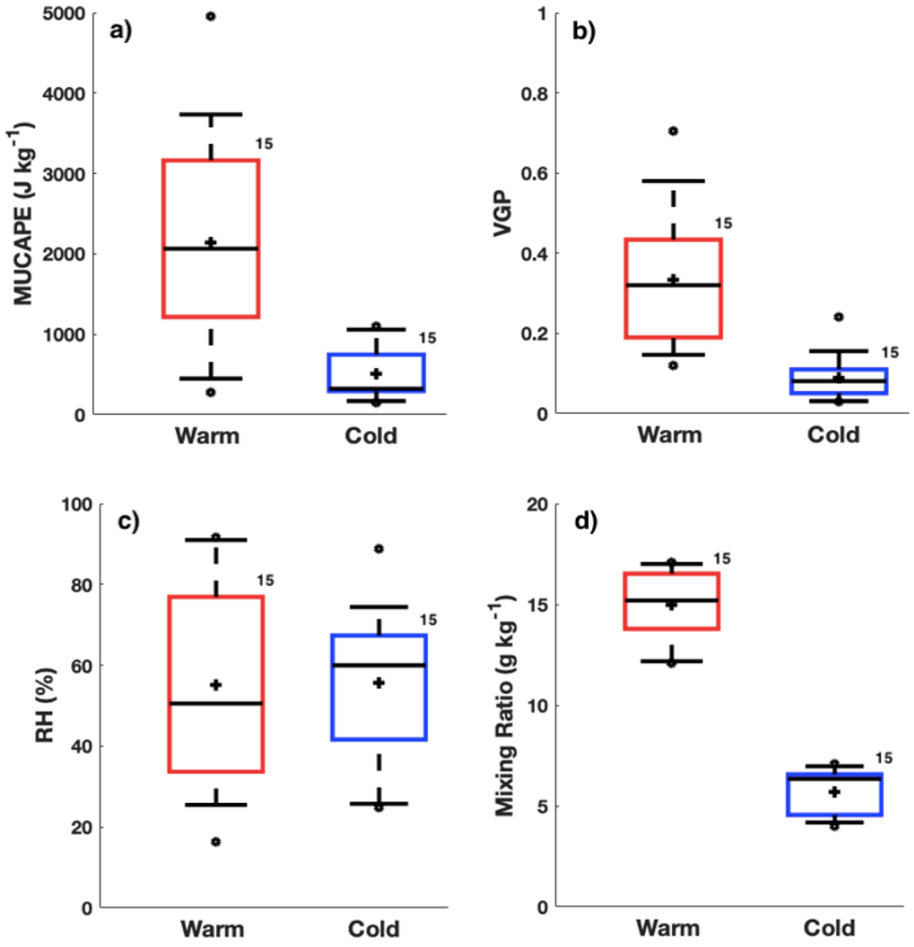

Figure 10. As in Figure 8, except for a comparison of a) MUCAPE, b) 0-3 km VGP, c) 3-6 km RH, and d) 100 mb ML mixing ratio.

b) Z_{DR} Columns

Z_{DR} columns were compared between the cold- and warm-based supercells to determine if there are any similarities and/or differences between the depth, areal extent, and the highest pixel values that characterize the columns. A direct comparison between the depth of the column and the environmental MUCAPE was also completed. All of the Z_{DR} column characteristic values were averaged over the whole observational period for the storms to produce a single representative value for each individual storm. The cold-based supercell cases only include three storms with an observable Z_{DR} column (Figure 11a), while the remainder (12 cases) had either enhanced Z_{DR} in the vertical that did not extend above the environmental 0°C level or did not exhibit any region of enhanced Z_{DR} above the lowest levels. All of the warm-based supercells exhibited a Z_{DR} column, and the deepest column observed among these cases reached 3.48 km above the environmental 0°C level.

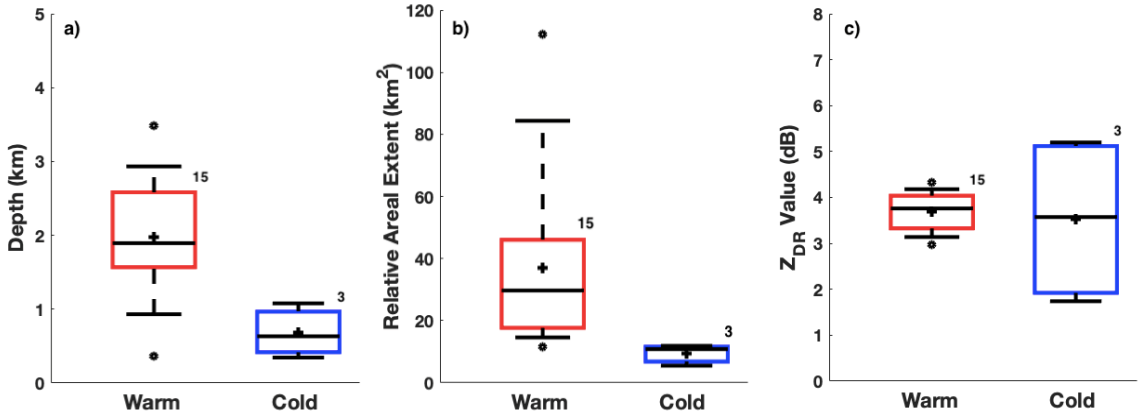

Figure 11. As in Figure 8, except for an analysis of the Z_{DR} column characteristics across environments, specifically focused on the a) 1-dB Z_{DR} column depth, b) the 0.5-dB Z_{DR} column areal extent at 1 km above the environmental 0°C level, and c) the 90th percentile of pixel values within the column areal extent region.

Column depths within the warm-based cases show large variation from the mean for all storms (standard deviation [σ]=0.78 km), with a maximum value of ~3.50 km and minimum depth of ~0.37 km. Variation within the observed column depths can possibly be explained by the highly variable MUCAPE observed within the warm-based supercell environments, along with the quantity of hail found within the two types of supercells. This sample of warm-based supercells tend to exist in higher MUCAPE environments than the cold-based supercells. Z_{DR} columns have been investigated in past literature and generally show a positive correlation with MUCAPE (Van Den Broeke 2016). Along with the analysis of MUCAPE, the height of the cloud base (using MLLCL or MLCCL as a proxy) can provide insight into what height the main updraft core would begin within the cloud, while the temperature profile above the MLLCL/MLCCL can provide further information about how deep the updraft may be. With warm-based supercells having relatively lower cloud bases (average cloud base ~0.54 km), the updrafts of these storm are likely deeper, where the cold-based supercells are more high-based in nature with a generally lesser updraft depth than the warm-based supercells. Since warm-based supercells are generally found in environments that have higher MUCAPE, lower cloud bases, and contain higher temperatures, deeper Z_{DR} columns were hypothesized and observed. ESRH within the warm-based environments is also relatively high. Since this variable is important for the ingestion of streamwise vorticity within the inflow layer of a storm leading to a potentially stronger rotating updraft, it could partially explain why these Z_{DR} columns are deeper than those observed in the cold-based supercells. The cold-based supercells are generally found in low ESRH environments compared to the warm-

based supercells (Figure 9e). These ESRH values are relatively small, leading to less ingestion of streamwise vorticity for supporting a strong rotating updraft.

The areal extent of the 0.5-dB Z_{DR} column at 1 km above the environmental 0°C level was also compared between the two sets of storms (Figure 11b). The areal extent of the Z_{DR} column can also indicate how broad or narrow the updraft is (Kumjian et al. 2010). The warm-based supercells show considerable variation of column areal extent, with averages ranging between 11.50 km^2 and 112.15 km^2. All warm-based cases also exhibit an observable areal extent of the 0.5 dB column (at 1 km above the 0 °C level) through part or all of the supercell's lifetime. Since most of the cold-based supercells did not exhibit a Z_{DR} column, those storms did not have an observable areal extent associated with a column. Most warm-based supercells exhibit column areal extents >20 km^2, likely indicating that these storms have tall updrafts that are rather broad. As observed with the depth of the column, the MUCAPE and ESRH are relatively high in warm-based environments, which provided a favorable environment for convection with strong rotating updrafts. ESHEAR in the direct inflow environment is also relatively high for the warm-based storms (Figure 9c). Although the mean environmental ESHEAR does not vary much between environments, the larger values in the warm-based supercell environments likely provide a more favorable environment for organized supercells with strong rotating updrafts, compared to the cold-based supercells that are relatively weaker.

The 90th percentile of pixel values observed in the 0.5-dB Z_{DR} column (the pixels analyzed are those within the 0.5 dB areal extent at 1 km above the environmental freezing level) was compared between cold- and warm-based environments (Figure 11c).

This can provide insight into the variation of drop size within the location where the areal extent was calculated, along with the updraft strength (Kumjian et al. 2010). If higher values of Z_{DR} are observed within this region, that is an indication that the updraft is strong enough to loft these larger raindrops or partially melted hail to higher altitudes. The highest pixel values within the warm-based columns vary between 2.90 and 4.40 dB, while maximum values in the cold-based supercell columns range between 2.10 and 6.0 dB. Storms that did not have any observable 0.5 dB column were considered "NA." Only three cold-based storms contribute to this range, although these storms provide results that contribute some of the highest pixel values. The higher Z_{DR} values indicate that the raindrops are more oblate, and therefore likely larger than the raindrops surrounding the column region. This shows that the updraft is strong enough to loft these larger raindrops to higher altitudes and is shown as an area of enhanced Z_{DR} (>2 dB for all cases) and is surrounded by smaller raindrops, graupel, or ice crystals that yield values near 0.0 dB. The fact that the cold-based storms exhibited some of the highest Z_{DR} pixel values is unexpected. Due to the lack of warm temperatures in the environments of these storms, it was not expected to find raindrops this large within the updraft, rather smaller less-oblate drops are expected. It is possible that partially/fully melted hail led to some of these large values. The higher amounts of moisture in the 3-6 km layer, evident through the pressure weighted RH in that layer, could lead to the production of larger drops through the shedding of liquid drops from the melting and recycling (water-soaked hail being lofted through the updraft) of small hail, leading to more efficient growth by collision-coalescence. The lower MUCAPE in the cold-based environments can indicate that there

may be lower vertical accelerations within the updraft and generally lower supersaturation, meaning that the raindrops would not grow as readily (Shaw 2000). Although raindrops may not grow as readily in cold-based environments, partially or fully melted hail would still yield very high Z_{DR} values, which indicates large liquid raindrops. The presence of melted ice crystals can also be contributing to these values. The opposite can be said about raindrops in higher MUCAPE environments, where the higher MUCAPE can indicate that there would be faster vertical accelerations within the updraft along with higher supersaturation, which would allow raindrops to grow to larger sizes. Since most of the warm-based storms are observed in higher MUCAPE environments, it is possible that this is the reason that the Z_{DR} pixel values varied less than those observed in the cold-based environments. Another factor that can be contributing to less variation in the pixel values can be lack of hail present within the warm-based supercells. With the presence of hail, values of Z_{DR} would either be large (if partially or fully melted) or near zero in the presence of large hail. Higher values found within the cold-based supercells are likely caused by the presence of melting hail, yielding very high Z_{DR}.

Pearson's correlation coefficient was calculated to determine if there was any correlation between MUCAPE and column depth, since MUCAPE is a metric used to determine potential updraft characteristics (Figure 12). There is a moderate positive correlation (R^2=0.5239) between the MUCAPE and Z_{DR} column depth. As the environmental MUCAPE increases, height of the observed Z_{DR} column generally increases also. Most of the cold-based storms occur in low MUCAPE environments, with

only one observed with MUCAPE >1000 J kg^{-1}. Storms in these low MUCAPE environments likely have relatively weak updrafts that are less capable of lofting large raindrops high enough to produce a column. Since the cold-based supercells are generally found in low MUCAPE environments, they are less likely to produce a Z_{DR} column. Cold-based supercells that did exhibit a column generally exhibited some high Z_{DR} values (>4 dB), as was discussed prior. The presence of more hail within the storms would likely lead to drop shedding, which would enhance the collision-coalescence process, increasing raindrop sizes more readily. A WMW test was also completed between the cold- and warm-based storms for each characteristic of the Z_{DR} column (Table 3). This test was conducted to see if different environments are responsible for the observed differences. This statistical test shows that the cold- and warm-based samples for both the column depth and areal extent had a large enough difference to be statistically distinguished. This means that the two data sets are not likely to come from the same population of storm types. The 90th percentile of the pixel values in the 0.5 dB column did not show large differences and could have been chosen from the same population of supercells. It is important to remember that only three cold-based storms contributed to the analysis for the 90th percentile since most of these storms did not exhibit a column.

Table 3. *P*-values for the Z_{DR} column characteristics.

Z_{DR} Column	
Comparison	**p-value**
Cold vs. Warm (Height)	2.98E-06
Cold vs. Warm (Area)	1.96E-06
Cold vs. Warm (90th Percentile)	4.26E-01

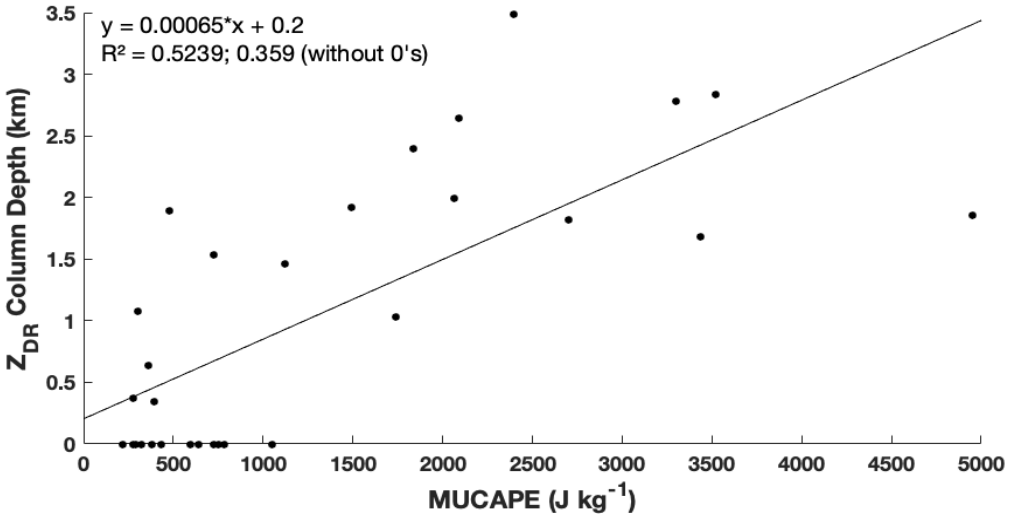

Figure 12. A comparison between the mean Z_{DR} column depth and the environmental MUCAPE for all supercell cases.

c. Low-Level Radar-Inferred Large Hail Signature

Characteristics of the Z_{DR} inferred hail core from the 1 -km CAPPIs were compared for cold- and warm-based supercells, specifically focused on the areal extent of the core, areal extent of the inferred hail core normalized by the size of the 35 dBZ echo, and the COV of the hail core size. These microphysical characteristics provide information regarding which environments may be more favorable for the development of large hail that may reach the ground. Since 1 km CAPPIs were utilized, storms exhibiting an inferred hail core are likely producing hail that is reaching the surface, as long as the low levels (below 1 km) were not warm enough to completely melt the hail. All supercell cases exhibited an inferred hail core, although many of the warm-based supercells have small areal extents of inferred hail. The warm-based supercells have average inferred hail core areas that range between 0.024 km^2 and 8.70 km^2, while the

cold-based supercells have hail cores that range between 1 km^2 and 50 km^2 (Figure 13a). Some warm-based supercells have very small average inferred hail core sizes, which can be attributed to many cases only exhibiting an observable hail core for part of the time period, while the time steps with no observable hail cores are recorded as "0 km^2." 80% of the cold-based supercells exhibited inferred hail cores that are larger than the largest observed inferred hail core within the warm-based supercells.

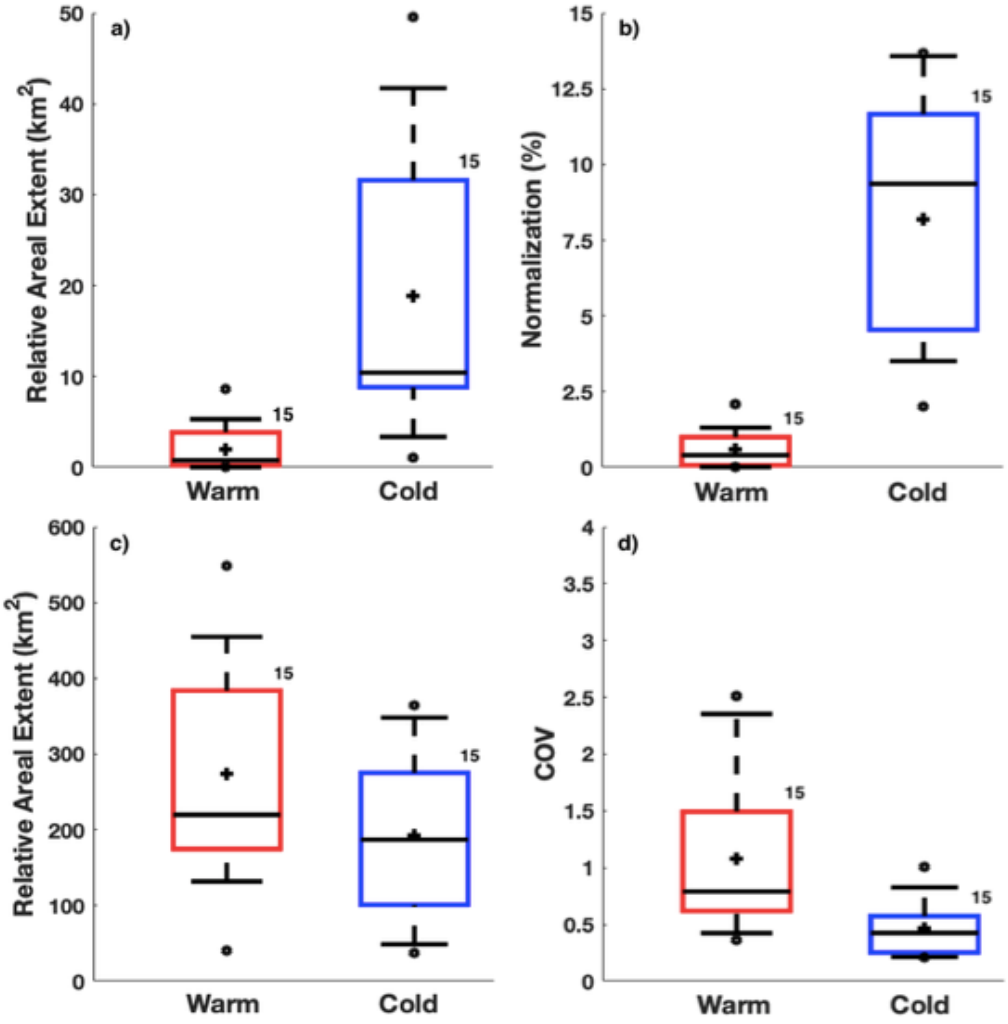

Figure 13. As in Figure 8, except for an analysis of the low-level Z_{DR} inferred hail core characteristics between environments, specifically focused on the a) areal extent of the inferred hail core, b) normalization of the hail core to the 35 dBZ core, c) areal extent of the 35 dBZ core, and d) COV of the areal extent of the hail core.

Table 4. *P*-values for the low-level Z_{DR} inferred hail core

Low-Level Z_{DR} Hail Core	
Comparison	**p-value**
Cold vs. Warm (Area)	3.51E-06
Cold vs. Warm (35 dBZ Normalization)	2.58E-08
Cold vs. Warm (COV)	1.20E-03
Cold vs. Warm 35 dBZ Area	1.40E-01

On average, the cold-based supercells had cloud bases that were at a higher altitude, compared to those observed in the warm-based environments. With relatively higher cloud bases in the cold-based environments, along with the thermal profiles being much cooler than those observed in the warm-based environments, the cloud bases in the cold-based environments would either be at or very close to the environmental 0 °C level. These cooler temperatures provide a favorable environment for the growth of hail relatively close to cloud base, compared to the warm-based environments in which raindrops would have to be lifted farther within the storm until they reach the 0 °C level. The presence of supercooled liquid drops is also an important factor in the growth of hail, especially in the lower levels, leading to growth by riming. The environmental 0 °C levels in the warm-based environments averaged ~3.8 km above ground level (AGL), while the 0 °C levels in the cold-based environments averaged ~2.4 km AGL. Since the formation of ice in the warm-based environments would generally start at higher levels, any hail in a warm-based storm also has a deeper warm/moist layer to fall through, which would likely cause more of the hail to melt before it reaches the 1 km level where the CAPPIs are constructed. The main factor leading to smaller inferred hail cores in the warm-based environments is likely due to the melting of hail, which would increase the Z_{DR} value beyond the Z_{DR} criterion required for a hail classification. The WMW *p*-value

calculated between supercell types indicates that they are likely from separate populations (Table 4).

The areal extent of the hail core was also normalized by the areal extent of the 35 dBZ reflectivity outline of each storm (Figure 13b). Since cold-based storms generally exhibited larger inferred hail cores on average, one could hypothesize that the percentage of inferred hail to the size of the 35 dBZ core would also be higher (compared to the warm-based cases). The size of the normalized core also varies greatly, ranging between 1% and 14% of the storm area (σ=3.73%). The warm-based storms varied much less, with a range of inferred hail between 0.0% and 2.1% (σ=0.58%). When comparing the two datasets, ~93% of the cold-based storms exhibit percentages of inferred hail that are larger than those observed in the warm-based storms. Similar environmental characteristics that may have been factors in the areal extent of the inferred hail core also likely influence the hail core normalization values, such as MUCAPE, 0 °C level, and the height of cloud base. This variable was also found to be statistically different between the two environments (Table 4). Along with this calculation, the spread of the areal extent of the 35 dBZ core between cases is shown (Figure 13c). Although some warm based supercells contributed to some of the largest 35 dBZ cores between environments, most of the core sizes fall within the same range of values between environments. Statistically, this metric is similar between environments (Table 4).

The COV was calculated by utilizing the raw hail core areal extent values for each case to understand the variation between cases in each environment. The warm-based supercells exhibit the most variation in hail core size, while the cold-based supercells

show less variation (Figure 13d). It was not uncommon to find warm-based supercells that exhibited little to no inferred hail core, and then a few time steps within the observational period that show a larger areal extent of inferred hail. This can lead to a larger variation, which can indicate that the storm is not consistently dropping hail (or in large enough concentrations) that is detected by radar throughout the whole observation period. The cold-based supercells generally show an observable hail core throughout most of the observation period. Warm-based supercells yield the highest median values with a median COV of 0.79, while the median COV for the cold-based supercells is 0.34. Since the medians between data sets are rather different, the WMW test also yielded a low *p*-value, indicating that these two samples are statistically different (Table 4). This can indicate that the warm-based supercells are either not continuously forming hail or the hail is melting before it reaches the elevation at which the radar sample was selected, leading to larger variation between time steps. Also, the cold-based supercells seem to continuously produce large quantities of hail, leading to less variation within the hail core size between time steps.

d. Z_{DR} Arcs

The Z_{DR} arc was the final polarimetric signature compared between the cold- and warm-based supercells. Specifically, the areal extent of the Z_{DR} arc and the 90^{th} percentile of the values found within the arc were compared to determine how this polarimetric signature is similar or different between the two different environments (Figure 14). Z_{DR} arcs can provide information regarding the size sorting processes occurring within the storms (e.g., Kumjian and Ryzhkov 2008). The areal extent of the Z_{DR} arcs had some

slight differences between environments, where the warm-based supercell areas range between 0.0 km^2 and 203 km^2 and the cold-based supercell areas ranged between 0.0 km^2 and 146 km^2 (Figure 14a). The WMW test indicates that, although the median values are quite different, the two sets of data are statistically similar (Table 5). The median arc areal extent in the warm-based supercells is 25.72 km^2, while the median for the cold-based supercells is 3.31 km^2. The average 90^{th} percentile of the pixel values found within the arc (for all pixels that meet the 2.5- and 3.5-dB thresholds within the arc) show some differences as well, where the warm-based supercells exhibit relatively similar Z_{DR} values with little variation compared to the cold-based supercells. Although the variation is not very large (Figure 14b), the cold-based storms show slightly larger variation from the mean (σ=1.02 dB), ranging between 3.9 dB and 6.8 dB, while the warm-based storms vary less (between 5 and 6.5 dB; σ=0.42 dB). This can indicate that the distributions of drops are slightly different between environments, with slightly larger raindrops possible in the cold-based supercell arcs (likely due to a broad distribution of raindrop sizes, including very large drops, because of partially or fully melted hail). Along with the standard deviations from the mean being rather high, the WMW test indicates that the two samples are statistically similar (p=0.12). Since these observed values are rather high in both environments, it is likely that partially or fully melted small hail is present within the arcs. A possible source of error can be due to the identification of the arcing features (especially in cold-based storms), since different thresholds were used for the Z_{DR} arcs between the environments (3.5 dB for warm-based storms and 2.5 dB for cold-based storms). The threshold for the cold-based supercells was lowered to account for the

number of cold-based storms that did not exhibit a 3.5-dB arc and because of the possible microphysical differences. Also, the 2.5 –dB arc better captured changes in the orientation of the arcs in cold-based cases, rather than the 3.5 dB threshold. Since cold-based storms are found in much cooler environments on average, the microphysical reasoning for lowering the threshold for the cold-based storms is to account for the higher concentrations of small hail and graupel that may not be melting and yielding lower Z_{DR} values in the arc region. It was also assumed that there would not be a large number concentration of large liquid raindrops due to the colder temperatures in the environmental profile. A large factor in the arcs found within the warm-based supercells can be the melting of hail, which would yield high $Z_{DR,}$ therefore exhibiting a Z_{DR} arc with many pixels exceeding the 3.5 dB threshold. There was likely some melting of hail within the cold-based supercells as well, which contributed to the larger arcs observed. There are seven of the cold-based supercells there are found in environments with a layer of wet bulb temperatures (T_w) > 5 ℃, which can indicate that there is partial/full melting of hail prior to reaching the 1 km CAPPI level. Although, the melting layer is less than 0.5 km deep for these cases. All warm-based supercells have layers in which T_w> 5 ℃ over a larger depth, leading to more melting of hail overall within this same region. The upper 90^{th} percentile of pixel values found within the cold-based arcs can indicate that there is a presence of smaller hail that is melting, yielding lower Z_{DR} values than that of large melting hail.

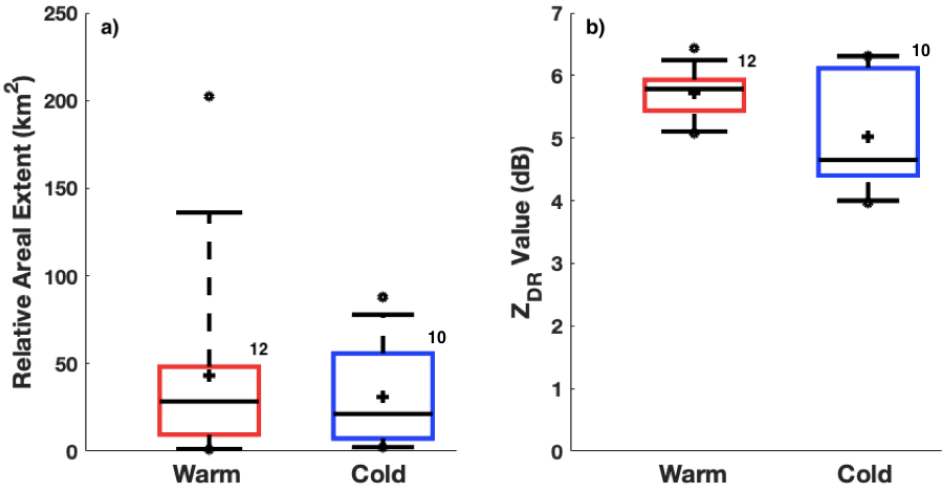

Figure 14. As in Figure 8, except for analysis of the Z_{DR} arc characteristics across environments, specifically focused on the a) areal extent of the 3.5- and 2.5-dB arc and b) 90th percentile of pixel values within the areal extent of the arc.

Environmental variables that have been investigated in prior literature (Kumjian and Ryzhkov 2009; Van Den Broeke 2016) which may influence the Z_{DR} arc characteristics include ESRH, ESHEAR, and MUCAPE. Pearson's correlation coefficient was calculated between the areal extent of the Z_{DR} arc and each of these environmental variables. Weak to no correlation was found between any of these environmental variables and the size of the Z_{DR} arc (Figure 15).

Table 5. *P*-values for the Z_{DR} arc characteristics

Z_{DR} Arc	
Comparison	***p*-value**
Cold vs. Warm (Area)	4.64E-01
Cold vs. Warm (90th Percentile)	9.31E-02

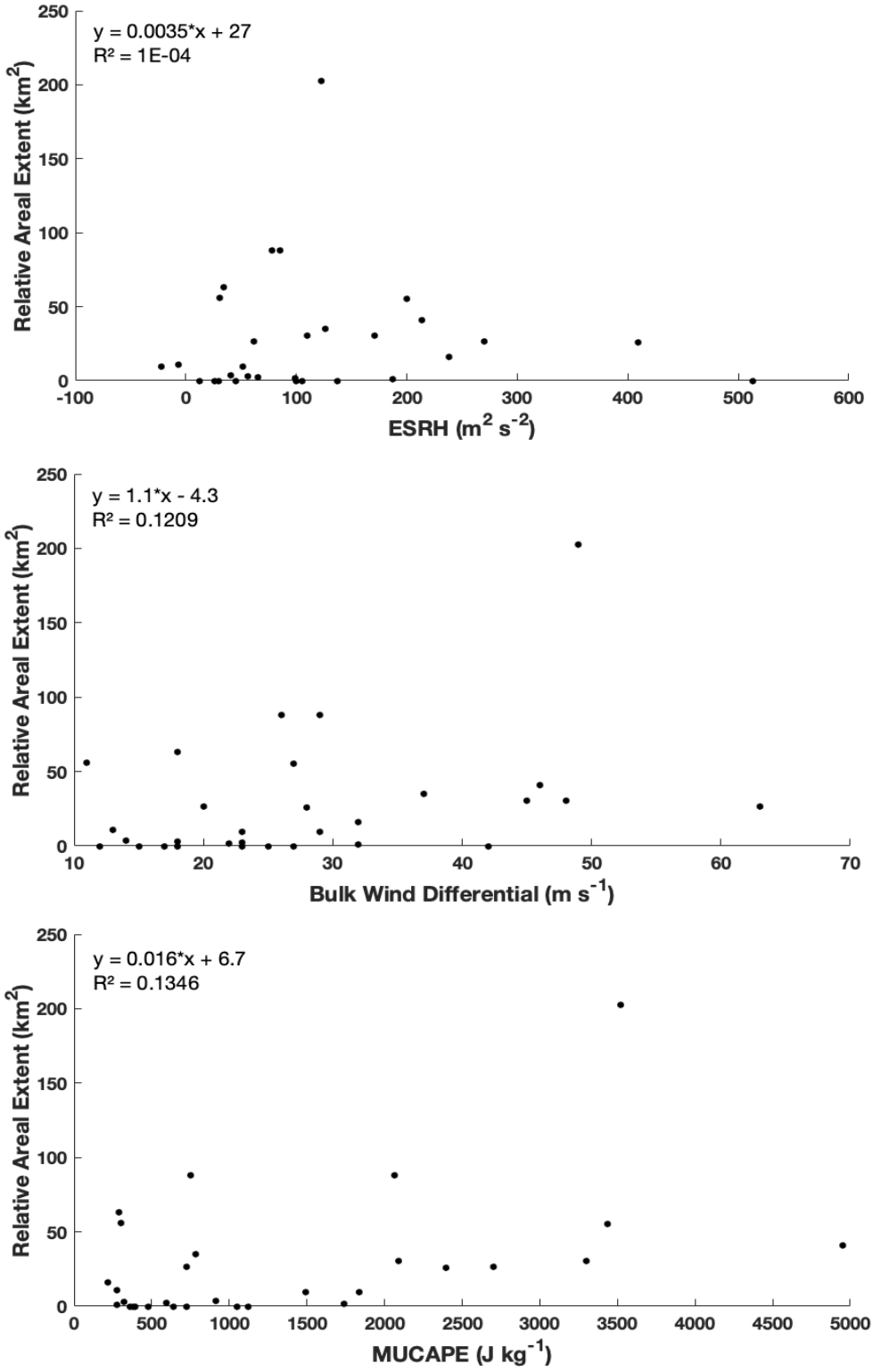

Figure 15. Scatterplots of the Z_{DR} arc area relative to a) ESRH, b) ESHEAR, and c) MUCAPE.

It would appear that the largest Z_{DR} arcs are generally associated with ESRH ranging from 0 $m^2 s^{-2}$ to 200 $m^2 s^{-2}$, while cases with ESRH beyond that range yield Z_{DR} arcs that are less than 50 km^2, although more cases would be needed to provide more meaningful conclusions (Figure 15a). Within this range, there is also a high amount of variability, where many of the cases exhibit near 0.0 km^2 areal extent. Similar findings resulted through the comparison with ESHEAR (Figure 15b). MUCAPE exhibited a slightly increasing trend (Figure 15c) when compared to the areal extent, although a larger sample size would be necessary to form any meaningful conclusions. This increasing trend can be partially due to the inclusion of the zeroes in the calculation of the R^2 value (0.2041). Without the zeroes included, the R^2 value decreases to 0.1346, indicating little to no correlation.

Results from the statistical analysis suggest that both characteristics showed little statistical significance, where the two samples generally seem as if they are gathered from a similar population of storms (Table 5). These results also indicate that the Z_{DR} arc does not change much as a function of environment, rather the dynamical size-sorting processes would have a stronger influence. It would seem that the Z_{DR} arc would correlate more with a dynamical difference, rather than microphysical differences resulting from their occurrence in different environments, since supercells are fairly similar dynamically (given the environments that are needed for their formation). This indicates that the Z_{DR} arc does not differ significantly between the two different environments.

5. Conclusions

Environmental conditions and polarimetric signatures were investigated for differences or similarities between supercell thunderstorms in warm- and cold-based environments. Warm-based supercells were found in environments with cloud base temperatures >15 ℃ (using MLLCL or MLCCL as a proxy), while the cold-based supercells were found in environments with cloud bases <5 ℃. The specific polarimetric signatures investigated were the Z_{DR} column, low-level Z_{DR} inferred hail core, and Z_{DR} arc. The characteristics and associated microphysical process responsible for these polarimetric signatures are relatively well known, although the characteristics of these signatures in differing environments are still not well understood (Kumjian and Ryzhkov 2008; Dawson et al. 2014; Van Den Broeke 2016).

Cold-based supercell thunderstorms were generally found in environments with much cooler temperature profiles. The cloud bases for these supercells were generally much higher, and more of these storms were high-based (> 1 km AGL). Since many of the storms had relatively high cloud bases, their cloud bases were already near the environmental 0 ℃ level, and some were <0 ℃. Cold-based environments were also typically low-MUCAPE environments. Thus, the VGP values were very low since this parameter relies heavily on the environmental CAPE. Shear and SRH were also relatively low within cold-based environments, which could help explain why these storms were relatively short-lived (generally less than a two-hour lifetime).

Z_{DR} column depth was relatively low for all cold-based supercells, and only four cases exhibited a Z_{DR} column. A possible factor leading to a lower Z_{DR} column depth is

the amount of instability (MUCAPE) found in these environments. Using all cases, there was a moderately positive correlation between Z_{DR} column depth and the MUCAPE. Since most cold-based supercells were found in low MUCAPE environments, the lower instability can indicate weaker vertical accelerations within the updraft core, leading to lower supersaturation and smaller raindrops. Along with MUCAPE, the environmental temperature can also play a role in the extent to which liquid water drops are found within the updraft. Since cold-based storms are found at or below the environmental 0 ℃ level, raindrops may begin to freeze and ice crystals may begin to form (e.g. Rogers and Yau 1989), yielding lower Z_{DR} values than liquid drops. Hallett and Mossop (1974) describe that drops generally begin to freeze between -3 °C and -8 °C, while rapid freezing is observed at temperatures below -8 °C. The introduction of ice crystals into the updraft core can lead to an overall lower mean Z_{DR} value found within. The areal extent of the Z_{DR} column (measured at 1 km above the environmental 0 ℃ level) yielded similar results, where the areal extents of the columns were fairly small. Both of these can indicate that the updrafts found within cold-based supercells do not extend very high and are relatively narrow. While there were only three cases that contributed to the 90th percentile of the pixel values within the 0.5 dB column, they contributed some of the highest values found within that region. These high Z_{DR} values can indicate the presence of partially or fully melted hail, or are just a consequence of drop shedding. The size of the shed drops depends on the size of the hailstone that is melting and shedding the drops (Rasmussen et al. 1984). The larger the hailstone, the larger the potential shed raindrop can be (Rasmussen et al. 1984). Rasmussen et al. (1984) mention that the drops shed

from melting hail can significantly alter the raindrop size distribution, which is potentially being observed in these cold-based supercells leading to larger Z_{DR} values. Rasmussen and Heymsfield (1987) later discuss that hailstones are known to shed 1 mm drops fairly frequently as they fall out of a storm (500 drops km^{-1}), which in turn, can lead to an enhancement in the amount of raindrops produced within a storm. These shed drops can also collide with other drops, possibly increasing the size of some drops in the process, broadening the drop size distribution (DSD) within the supercells.

The areal extent of the low-level Z_{DR} inferred hail core within the cold-based supercells was relatively large for most cases, with an average area of 19.1 km^2. On average, the area normalization by the 35 dBZ reflectivity core was also rather large, indicating that a larger percentage of the reflectivity core is dominated by hail. The much colder air within these storms is likely a large factor in the amount and persistence of hail found within these storms. With cooler temperatures, there is likely less melting, yielding larger hail that is relatively dry (yielding Z_{DR} ~0.0 dB within the core). The COV for the cold-based supercells was generally low (<1), indicating that there was not a large variation in the inferred hail core's areal extent. The spread of the COV was also rather low. This can indicate that the hail cores within the cold-based supercells do not show much variation in size between time steps, indicating that the storm has a generally consistent hail core throughout the observational period. Not only does this signature infer the presence of hail, it also indicates that there are likely large and dry hailstones present in the lower levels of the storm, which are likely reaching the surface. The Z_{DR} arc was the final polarimetric signature investigated. The statistical analysis between

environments indicates that the two sets of storms are statistically similar, where the storms could have been pulled from a similar environment. There was a larger variation in the 90th percentile of pixel values within the arcs in the cold-based cases, although the median values were statistically similar.

Warm-based supercells were found in environments with much warmer temperature profiles. While the cold-based supercells were typically high-based, only two of the warm-based supercells exhibited cloud bases >1 km. Since many of the warm-based supercells had warmer temperature profiles than the cold-based storms, their environmental 0 ℃ levels were also relatively higher than those found in the cold-based environments. MUCAPE for the warm-based supercells was also >1000 J kg^{-1} for all cases. The higher MUCAPE in the environments and the warmer temperature profiles both provided favorable conditions for strong updrafts. The VGP, as mentioned prior, heavily relies on the environmental CAPE. Therefore, VGP values were also relatively high in warm-based supercell environments, indicating a higher rate of vorticity stretching and tilting near the updraft (favoring stronger rotation). Both low-level and deep-layer shear were higher in the warm-based supercells, which likely helped to maintain the supercells and allow them to be longer-lived than the cold-based supercells. Along with the shear, SRH and ESRH were also high for the warm-based supercells, which likely helped the supercells ingest more streamwise vorticity into the updraft, enhancing rotation and storm longevity.

All warm-based supercells exhibited a Z_{DR} column, where the depth of these columns were generally large for most of the storms. The large Z_{DR} column depths are

likely attributable to the warmer temperature profile and higher instability (MUCAPE) found within the warm-based environments, which favor strong and persistent updrafts. The Z_{DR} column depth had a positive correlation with MUCAPE, where environments with higher MUCAPE generally exhibited supercells with large Z_{DR} column depths. Along with warm-based supercells exhibiting deeper Z_{DR} columns, the 0.5 dB areal extents of the columns were also large compared to the cold-based storms. The large areal extents can be used to infer that the updrafts within warm-based supercells were relatively broad. Microphysically, this can indicate that there is a larger presence of oblate liquid raindrops, where partially or fully melted hail can also yield similar values within this region. The 90^{th} percentile of pixel values observed in the 0.5 dB areal extent were relatively high (3-5 dB), while the cold-based supercells exhibited even higher values. These higher values can be indicative of partially or fully melted hail. Since there were not high concentrations of hail found in the warm-based storms, this may be a factor in why the Z_{DR} values were not as high as those observed in cold-based supercells, where there was a large quantity of hail that was likely partially or fully melted. Warm-based supercells show little to no Z_{DR} inferred hail at the lowest radar elevation scan. The areal extent of the inferred hail for the warm-based cases is much lower than the hail cores observed in the cold-based supercells. A factor leading to this significant difference is likely the warmer thermal profiles observed in the warm-based environments, providing favorable conditions to melt any hail before it reaches ~1 km AGL (the altitude of the CAPPIs used). Since the inferred hail core was near 0.0 km^2, the normalization by the 35 dBZ radar reflectivity core also yielded very small percentages of hail to the reflectivity

core. The COV was relatively high within the warm-based supercells, likely because storms may not have larger/dry hail falling through the scanning elevation continuously. A few time steps would indicate an inferred hail core (mainly smaller areas), while most would show no inferred hail. This would increase the COV for each case, which could indicate that much of the hail forming aloft is likely melting before it reaches the CAPPI altitude. There were no large statistical differences between the areal extent of the Z_{DR} arcs of the cold- and warm-based supercells. The 90th percentile of pixel values in the warm-based supercells shows less variation between cases. When Pearson's correlation coefficient was calculated between the shear, SRH, and MUCAPE, there was little to no correlation with the size of the arc to the environmental characteristics. The MUCAPE shows a slightly increasing trend, yet it was a rather small value (R^2=0.21). These results indicate that the characteristics of the Z_{DR} arc have less of an influence from the microphysical properties/processes, rather dynamical processes likely are more of a factor.

Overall, most of the polarimetric signatures indicated some differences within different environmental constraints. The features that showed the most significant differences between environments were the Z_{DR} column depths and the low-level Z_{DR} inferred hail core areas. The main environmental factors that seem to influence these characteristics are the MUCAPE and the thermal profiles. Cold-based supercells were found in environments with much cooler temperature profiles, where much of the storm is below freezing. The colder temperature profile can promote the continuous formation of hail, which was evident through the analysis of the inferred Z_{DR} hail core. While these

environmental characteristics show differences across environments, the Z_{DR} arc showed little to no differences between environments. A possible implication in the calculation of the Z_{DR} arcs would be the different thresholds utilized between environments. These thresholds were utilized due to the lack of observable Z_{DR} arcs in the cold-based supercells when using the 3.5 dB threshold, along with microphysical differences in the storms, such as the presence of small hail or graupel (yielding near 0 dB returns). Overall, this research will provide some useful information regarding different polarimetric signatures associated with supercells in certain environments, and will assist in better nowcasting the potential hazards that could be anticipated with a given scenario. The height and temperature of cloud base are a quick way to identify the type of supercell (warm- or cold-based) that can be expected, although the environments are quite distinct between each supercell type. Understanding these environmental differences can aid in better hazard forecasting and messaging. Specifically, analyzing the amount of low-level moisture, instability, height of the environmental 0 °C level, and the overall temperature profile can provide some vital information regarding the potential orientation of these polarimetric signatures that may be observed, along with the microphysical significance behind these orientations. This investigation will also be useful to research meteorologists since there are many other polarimetric signatures that have yet to be investigated between these two very different environments defined by cloud base temperature. Future work will investigate these types of supercells with a larger dataset, along with analyzing which type of supercell is most favorable for the development of tornadoes and how these signatures may differ between tornadic and nontornadic supercells.

6. References

Balakrishnan, N. and D.S. Zrnić, 1990: Use of polarization to characterize precipitation and discriminate large hail. *J. Atmos. Sci.*, **47**, 1525-1540, https://doi.org/10.1175/1520-0469(1990)047<1525:UOPTCP>2.0.CO;2

Brown, R.A., 1992: Initiation and evolution of updraft rotation within an incipient supercell thunderstorm. *J. Atmos. Sci.*, **49**, 1997–2031, https://doi.org/10.1175/1520-0469(1992)049<1997:IAEOUR>2.0.CO;2

Browning, K.A. and R.J. Donaldson, 1963: Airflow and structure of a tornadic storm. *J. Atmos. Sci.*, **20**, 533–545, https://doi.org/10.1175/1520-0469(1963)020<0533:AASOAT>2.0.CO;2

Browning, K. A., 1986: Morphology and classification of middle-latitude thunderstorms. Chapter 7, Thunderstorm Morphology and Dynamics. E. Kessler, Ed., University of Oklahoma Press, 133-152.

Bunkers, M.J., B.A. Klimowski, J.W. Zeitler, R.L. Thompson, and M.L. Weisman, 2000: Predicting supercell motion using a new hodograph technique. *Wea. Forecasting*,**15**, 61–79, https://doi.org/10.1175/1520-0434(2000)015<0061:PSMUAN>2.0.CO;2

Bunkers, M.J., M.R. Hjelmfelt, and P.L. Smith, 2006a: An observational examination of long-lived supercells. Part I: Characteristics, evolution, and demise. *Wea. Forecasting,* **21**, 673–688, https://doi.org/10.1175/WAF949.1

Bunkers, M.J., J.S. Johnson, L.J. Czepyha, J.M. Grzywacz, B.A. Klimowski, and M.R. Hjelmfelt, 2006b: An observational examination of long-lived supercells. Part II: Environmental conditions and forecasting. *Wea. Forecasting,* **21**, 689–714, https://doi.org/10.1175/WAF952.1

Burgess, D. W., V. T. Wood, and R. A. Brown, 1982: Mesocyclone evolution statistics. Preprints, *12th Conf. Severe Local Storms*. Amer. Meteor. Soc., 422-424.

Carbone, R. E., J. W. Conway, N. A. Crook, and M. W. Moncrieff, 1990: The generation and propagation of a nocturnal squall line. Part I: Observations and implications for mesoscale predictability. Mon. Wea. Rev., **118**, 26–49, doi:10.1175/ 1520-0493(1990)118,0026:TGAPOA.2.0.CO;2.

Chrisman, J. N., 2014: The continuing evolution of dynamic scanning. NEXRAD Now, No. 23, NOAA/NWS/Radar Operations Center, Norman, OK, 8–13.

Colman, B.R., 1990a: Thunderstorms above Frontal Surfaces in Environments without Positive CAPE. Part I: A Climatology. *Mon. Wea. Rev.,* **118**, 1103–1122, https://doi.org/10.1175/1520-0493(1990)118<1103:TAFSIE>2.0.CO;2

Colman, B.R., 1990b: Thunderstorms above Frontal Surfaces in Environments without Positive CAPE. Part II: Organization and Instability Mechanisms. *Mon. Wea. Rev.,***118**, 1123–1144, https://doi.org/10.1175/1520-0493(1990)118<1123:TAFSIE>2.0.CO;2

Conway, J. W., and D. S. Zrnic´, 1993: A study of production and hail growth using dual-Doppler and multiparameter radars. *Mon. Wea. Rev.,* **121,** 2511–2528, https://doi.org/10.1175/1520-0493(1993)121<2511:ASOEPA>2.0.CO;2

Crowe, C. C., C. J. Schultz, M. Kumjian, L. D. Carey, and W. A. Petersen, 2012: Use of dual-polarization signatures in diagnosing tornadic potential. *Electron. J. Oper. Meteor.*, **13 (5)**. [Available online at http://www.nwas.org/ej/pdf/2012-EJ5.pdf.]

Dawson, D.T., E.R. Mansell, Y. Jung, L.J. Wicker, M.R. Kumjian, and M. Xue, 2014: Low-level z_{dr} signatures in supercell forward flanks: The role of size sorting and melting of hail. *J. Atmos. Sci.,* **71**, 276–299, https://doi.org/10.1175/JAS-D-13-0118.1

Dawson, D.T., E.R. Mansell, and M.R. Kumjian, 2015: Does wind shear cause hydrometeor size sorting?. *J. Atmos. Sci.,* **72**, 340–348, https://doi.org/10.1175/JAS-D-14-0084.1

Dessens, J. and J.T. Snow, 1989: Tornadoes in France. *Wea. Forecasting,* **4**, 110–132, https://doi.org/10.1175/1520-0434(1989)004<0110:TIF>2.0.CO;2

Donaldson, R.J., 1970: Vortex Signature Recognition by a Doppler Radar. *J. Appl. Meteor.*, **9**, 661–670, https://doi.org/10.1175/1520-0450(1970)009<0661:VSRBAD>2.0.CO;2

Ferrier, B.S. and R.A. Houze, 1989: One-dimensional time-dependent modeling of GATE cumulonimbus convection. *J. Atmos. Sci.*, **46**, 330–352, https://doi.org/10.1175/1520-0469(1989)046<0330:ODTDMO>2.0.CO;2

Hallett, J. and S. Mossop, 1974: Production of secondary ice particles during the riming process. *Nature*, **249,** 26–28, https://doi.org/10.1038/249026a0

Heinselman, P.L. and A.V. Ryzhkov, 2006: Validation of polarimetric hail detection. *Wea. Forecasting,* **21**, 839–850, https://doi.org/10.1175/WAF956.1

Hubbert, J., V.N. Bringi, L.D. Carey, and S. Bolen, 1998: CSU-CHILL polarimetric radar measurements from a severe hail storm in eastern colorado. *J. Appl. Meteor.,* **37**,749–775, https://doi.org/10.1175/1520-0450(1998)037<0749:CCPRMF>2.0.CO;2

Iowa State University, Iowa Environmental Mesonet (IEM), 2020: Rapid Refresh and Rapid Update Cycle Model Sounding Archive. Accessed February 2020. [Available online at https://mtarchive.geol.iastate.edu/?C=D;O=A]

Klemp, J.B., R.B. Wilhelmson, and P.S. Ray, 1981: Observed and numerically simulated structure of a mature supercell thunderstorm. *J. Atmos. Sci.,* **38**, 1558–1580, https://doi.org/10.1175/1520-0469(1981)038<1558:OANSSO>2.0.CO;2

Kumjian, M.R. and A.V. Ryzhkov, 2008: Polarimetric signatures in supercell thunderstorms. *J. Appl. Meteor. Climatol.,* **47**, 1940–1961, https://doi.org/10.1175/2007JAMC1874.1

Kumjian, M.R. and A.V. Ryzhkov, 2009: Storm-relative helicity revealed from polarimetric radar measurements. *J. Atmos. Sci.,* **66**, 667–685, https://doi.org/10.1175/2008JAS2815.1

Kumjian, M.R., A.V. Ryzhkov, V.M. Melnikov, and T.J. Schuur, 2010: Rapid-scan super-resolution observations of a cyclic supercell with a dual-polarization WSR-88D.*Mon. Wea. Rev.,* **138**, 3762–3786, https://doi.org/10.1175/2010MWR3322.1

Kumjian, M.R. and A.V. Ryzhkov, 2012: The impact of size sorting on the polarimetric radar variables. *J. Atmos. Sci.,* **69**, 2042–2060, https://doi.org/10.1175/JAS-D-11-0125.1

Lemon, L. R., 1977: New severe thunderstorm radar identification techniques and warning criteria: A preliminary report. NOAA Tech. Memo. NWS-NSSFC 1, 60 pp. [NTIS No. PB-273049.]

Lemon, L.R. and C.A. Doswell, 1979: Severe thunderstorm evolution and mesocyclone structure as related to tornadogenesis. *Mon. Wea. Rev.*, **107**, 1184–1197, https://doi.org/10.1175/1520-0493(1979)107<1184:STEAMS>2.0.CO;2

MacIntosh, C.W. and M.D. Parker, 2017: The 6 May 2010 elevated supercell during VORTEX2. *Mon. Wea. Rev.*, **145**, 2635–2657, https://doi.org/10.1175/MWR-D-16-0329.1

Markowski, P., & Richardson, Y. P. (2010). *Mesoscale meteorology in midlatitudes*. Oxford: Wiley-Blackwell, 658 pp.

Marwitz, J.D., 1972: The structure and motion of severe hailstorms. Part I: Supercell storms. *J. Appl. Meteor.*, **11**, 166–179, https://doi.org/10.1175/1520-0450(1972)011<0166:TSAMOS>2.0.CO;2

Moller, A.R., C.A. Doswell, M.P. Foster, and G.R. Woodall, 1994: The operational recognition of supercell thunderstorm environments and storm structures. *Wea. Forecasting*, **9**, 327–347, https://doi.org/10.1175/1520-0434(1994)009<0327:TOROST>2.0.CO;2

Moore, J. T., A. C. Czarnetzki, and P. S. Market, 1998: Heavy precipitation associated with elevated thunderstorms formed in a convectively unstable layer aloft. *Meteor. Appl.*, **5**, 373– 384, doi:10.1017/S1350482798000863.

NCEI, 2019: Weather and Climate Toolkit, version 4.2.0. Accessed March 2019, [Available online at https://www.ncdc.noaa.gov/wct/index.php]

NOAA, 2018: Warning Decision Training Devision (WDTD). Accessed July 2019, [Available online at https://training.weather.gov/wdtd/]

NOAA, 2019: BUFKIT, version 18. Accessed February 2020, [Available online at https://training.weather.gov/wdtd/tools/BUFKIT/]

Palmer, R.D., D. Bodine, M. Kumjian, B. Cheong, G. Zhang, Q. Cao, H.B. Bluestein, A. Ryzhkov, T. Yu, and Y. Wang, 2011: Observations of the 10 May 2010 tornado outbreak using OU-Prime: Potential for new science with high-resolution polarimetric radar. *Bull. Amer. Meteor. Soc.*, **92**, 871–891, https://doi.org/10.1175/2011BAMS3125.1

Parker, M.D., 2014: Composite VORTEX2 supercell environments from near-storm soundings. *Mon. Wea. Rev.*, **142**, 508–529, https://doi.org/10.1175/MWR-D-13-00167.1

Picca, J. and A. Ryzhkov, 2012: A dual-wavelength polarimetric analysis of the 16 May 2010 Oklahoma City extreme hailstorm. *Mon. Wea. Rev.*, **140**, 1385–1403, https://doi.org/10.1175/MWR-D-11-00112.1

Pointin, Y., D. Ramond, and J. Fournet-Fayard, 1988: Radar differential reflectivity z_{dr}: A real-case evaluation of errors induced by antenna characteristics. *J. Atmos. Oceanic Technol.*, **5**, 416–423, https://doi.org/10.1175/1520-0426(1988)005<0416:RDRARC>2.0.CO;2

QGIS, 2019: version 3.8. Accessed January 2020, [Available online at https://www.qgis.org/en/site/]

Rasmussen, R.M., V. Levizzani, and H.R. Pruppacher, 1984: A wind tunnel and theoretical study on the melting behavior of atmospheric ice particles: Part. III. Experiment and theory for spherical ice particles of radius > 500 μm. *J. Atmos. Sci.*, **41**, 381–388, https://doi.org/10.1175/1520-0469(1984)041<0381:AWTATS>2.0.CO;2

Rasmussen, R.M. and A.J. Heymsfield, 1987: Melting and shedding of graupel and hail. Part III: Sensitivity study. *J. Atmos. Sci.*, **44**, 2764–2782, https://doi.org/10.1175/1520-0469(1987)044<2764:MASOGA>2.0.CO;2

Rasmussen, E.N. and D.O. Blanchard, 1998: A Baseline Climatology of Sounding-Derived Supercell and Tornado Forecast Parameters. *Wea. Forecasting*, **13**, 1148–1164,https://doi.org/10.1175/1520-0434(1998)013<1148:ABCOSD>2.0.CO;2

Rinehart, R. E., 2010: Radar for meteorologists. Rinehart Publications, 482 pp.

Rotunno, R., J. B. Klemp, and M. L. Weisman, 1988: A theory for strong, long- lived squall lines. J. Atmos. Sci., **45**, 463–485, doi:10.1175/ 1520-0469(1988)045,0463:ATFSLL.2.0.CO;2.

Ryzhkov, A. and D. Zrnić, 1996: Assessment of Rainfall Measurement That Uses Specific Differential Phase. *J. Appl. Meteor.*, **35**, 2080–2090, https://doi.org/10.1175/1520-0450(1996)035<2080:AORMTU>2.0.CO;2

Seliga, T.A. and V.N. Bringi, 1976: Potential use of radar differential reflectivity measurements at orthogonal polarizations for measuring precipitation. *J. Appl. Meteor.,***15**, 69–76, https://doi.org/10.1175/1520-0450(1976)015<0069:PUORDR>2.0.CO;2

Shaw, R.A., 2000: Supersaturation intermittency in turbulent clouds. *J. Atmos. Sci.*, **57**, 3452–3456, https://doi.org/10.1175/1520-0469(2000)057<3452:SIITC>2.0.CO;2

Thompson, R.L., R. Edwards, J.A. Hart, K.L. Elmore, and P. Markowski, 2003: Close proximity soundings within supercell environments obtained from the rapid update cycle. *Wea. Forecasting,* **18**, 1243–1261, https://doi.org/10.1175/1520-0434(2003)018<1243:CPSWSE>2.0.CO;2

Van Den Broeke, M.S., J.M. Straka, and E.N. Rasmussen, 2008: Polarimetric radar observations at low levels during tornado life cycles in a small sample of classic southern plains supercells. *J. Appl. Meteor. Climatol.,* **47**, 1232–1247, https://doi.org/10.1175/2007JAMC1714.1

Van Den Broeke, M.S., 2016: Polarimetric variability of classic supercell storms as a function of environment. *J. Appl. Meteor. Climatol.,* **55**, 1907–1925, https://doi.org/10.1175/JAMC-D-15-0346.1

Van Den Broeke, M.S., 2017: Polarimetric radar metrics related to tornado life cycles and intensity in supercell storms. *Mon. Wea. Rev.*, **145**, 3671–3686, https://doi.org/10.1175/MWR-D-16-0453.1

Wilks, D. A., 2006: *Statistical Methods in the Atmospheric Sciences*. 2nd ed. Academic Press, 627 pp.